EFFICIENT ALGORITHM FOR CALCULATION OF RADAR CROSS SECTION

Final Report

Sponsored by

Defense Advanced Research Project Agency (DOD)
Defense Small Business Innovative Research Program
ARPA Order No. 5916, Audit 9
Issued by U.S. Army Missle Command Under
Contract #DAAHO1-88-C-0863

Prepared by

InterScience, Inc.
105 Jordan Road
Troy, NY 12180
Tel. (518)-283-7500

Effective Date of Contract
September 26, 1988

Contract Expiration Date
March 27, 1989

EFFICIENT ALGORITHM FOR CALCULATION OF RADAR CROSS SECTION

Eduardo Saravia
D. Marc Audet
James F. Pipkins
Betriz Cassis
Robert Cole
James T. Woo (Principal Investigator)

InterScience, Inc.
105 Jordan Road
Troy, NY 12180

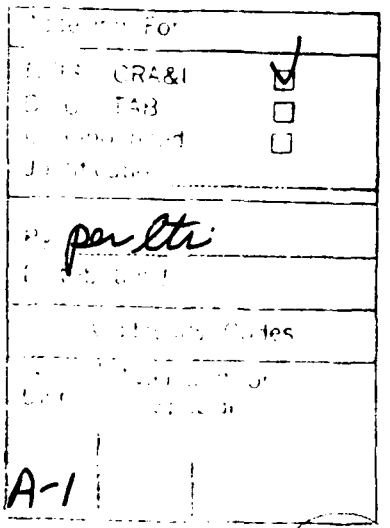

DISCLAIMER

"The views and conclusions contained in this document are those of authors and should not be interperted as representing the official policies, either expressed or imnplied of the Defense Advanced Research Project Agency or the U.S Goveronment".

EXECUTIVE SUMMARY

A new formulation for the calculation of radar cross section of objects of arbitrary shape based on the solution of the electromagnetic wave equation in a natural coordinate system that conforms to the shape of the boundaries has been developed. The natural coordinate system is determined from the solution of an elliptical partial differential equation subject to Dirichlet boundary conditions. The basic approach is to solve the electromagnetic wave equation expressed in the natural coordinate system in a region between the scattering object and an fictitious interface that fully envelopes the object (a circle for two dimensional objects and a sphere for three dimensional objects). Outside the interface, the wave field can be expressed as infinite series of Bessel types of functions. A unique solution is obtained by matching the boundary conditions at the fictitious interface.

Under the six-months DOD/SBIR Phase I Program funded by DARPA , the development of an algorithm based on this formulation to calculate the radar cross section of two dimensional objects to demonstrate the advantages of this approach has been successfully carried out. The formulation is completely general and can be extended to analyze the radar cross section of three dimensional objects. By using the natural coordinate system, it is also possible to analyze the radar cross section of objects of composite structure that can be represented by nested surfaces of arbitrary shapes.

Extensive benchmark calculations have been carried out using the code. Comparison with analytical solutions for scattering off simple objects showed excellent agreement to less than 1% error with relatively trivial computational requirements and effort. Results of calculated radar cross

section for ellipses, rectangles and crosses are compared to show their distinctly different signatures. The availability of such a code capable of efficient and accurate calculation of radar cross sections can be expected to have application to defense programs in three important areas. The first is for use in interactive design of flight vehicles to rapidly evaluate different design options. The second is for use in interactive design of detection facilities for maximum sensitivity and discrimination capabilities. Thirdly, with further refinements to the code and advances in computer hardware, it should be possible to implement a system on manned and unmanned flight and space vehicles with capability for on-line processing of radar signals for more selective targeting and defensive manuvers.

TABLE OF CONTENTS

I. INTRODUCTION

The ability to calculate accurately the radar cross section of objects of arbitrary shape with complex composite structures is of interest to defense programs for a variety of reasons. In the design of flight vehicles with minimum radar cross sections, it is desirable to be able to interactively evaluate the design options by numerical analysis before committing to hardware modeling studies. For the design of detection systems, it is equally important to be able to determine the response of various types of threats in order to properly configure the detection systems. In general, both monostatic cross sections of backscattered waves and multi-static cross sections as seen by remote receivers are of interest.

In general, the radar cross section of an object can be determined from the solution of the electromagnetic wave equation subject to the boundary conditions at the surface of the scattering object. For objects of very simple shape, such as spheres and infinite cylinders, analytical solutions exist from which the differential radar cross sections at any scattering angle can be determined. In the more general case, the solutions can be found only by numerical techniques. Furthermore, for complex, three dimensional objects with composite structures, numerical solutions by a brute force approach can be taxing for even the most advanced computers and they are not well suited for interactive or field usage. Therefore, there is the need for more efficient algorithms for the accurate solution of Maxwell's equations.

In recognition of such needs, we have developed a significantly more efficient approach for the solution of Maxwell's equations to calculate radar cross section of three dimensional objects of arbitrary shape and composition.

A feature of the approach is the possibility to analyze the response from nested surfaces of composite structures. With support from the Defense Advanced Research Project Agency (DARPA) under the 1988 DOD/SBIR Phase I program, we have developed a formulation of this approach to demonstrate its capabilities.

In the spirit of the SBIR program, which specifies that the objective of the Phase I program is to establish insofar as possible, the scientific or technical merit and feasibility of the idea, we limited our objective of the six-month Phase I effort to developing the algorithm for calculating the cross section for the scattering of electromagnetic waves from infinitely conducting surfaces of arbitrary two- dimensional shapes. The formulation can then be generalized for treating scattering from fully three-dimensional objects with composite structures under the more extended Phase II efforts. The results of the Phase I effort is fully described in this Phase I Final Report. The mathematical concept underlying our approach is described in Section II. Details of the formulation and the algorithms for solutions can be found in the Appendices. Examples of results from benchmark calculations are presented in Section III. Conclusions regarding the demonstrated and projected capabilities of the methodology are discussed in Section IV.

II. MATHEMATICAL CONCEPT

The basic problem we want to address is to solve the electromagnetic wave equation in infinite space, subject to boundary conditions imposed by the scattering object of arbitrary shape in which the material parameters may be inhomogeneous and anisotropic with sharp discontinuities. It is intuitively obvious that the accuracy of the

solution is critically dependant on the proper representation of the shape of the scattering object in the computational grid used for the numerical solution. For objects with a composite structure, such shapes constitute a nested sets of surfaces. Therefore, accurate representation of arbitrary shapes by a brute force technique would require the use of a very fine grid which can be computationally demanding.

To avoid this difficulty, we formulate the electromagnetic wave scattering problem in a natural coordinate system that conforms to the arbitrary shapes of the nested series of surfaces. Far away from the scattering object, we can also expect the effects due to the detailed features of the scattering surfaces to be smoothed out and it should then be possible to solve the wave equations on a more conventional grid. To minimize the computational efforts, we divide the infinite space into two regions separated by a fictitious boundary that fully encloses the scattering object (or circle for a two dimensional object). Inside the fictitious interface, we solve the wave equations in the natural coordinate system. Near the interface, the natural coordinate system gradually conforms to the shape of the interface. Outside of the interface, the wave equation can be solved in a conventional coordinate system in which the functional form of the solution is known and the boundary conditions are simple. A unique solution is then obtained by matching the two solutions at the fictitious interface. By using this approach, we are able to achieve higher accuracy with less computational effort.

Following this approach, the method of solution consists of several steps. The first step is to generate the natural coordinate system in the multiply connected region between the scattering object and the fictitious interface. We then rewrite the electromagnetic wave equation in this new

coordinate system. Because of the arbitrary shape of the scattering object, the boundary conditions are complicated. which will be governed by simple boundary conditions. However, the natural coordinate system leads to simple boundary conditions and the wave equation can be easily solved numerically in the transformed region. Outside the fictitious interface, the solution can always be represented by a harmonic series. The amplitudes of each of the harmonics is determined by matching to the interior solution at the fictitious interface.

For the Phase I effort, we restrict ourselves to address the two dimensional problem of calculating the scattering cross section for infinite rods of arbitrary but constant cross sectional shape. We chose as the fictitious interface an infinite cylinder of radius **a** that fully surrounds the scattering object and defines a doubly connected interior region as shown in Fig. 1. We shall use the axis of the infinite cylinder as the origin of a cylindrical reference system (r,ϕ) with the ignorable coordinate z along the axis of this fictitious cylinder.

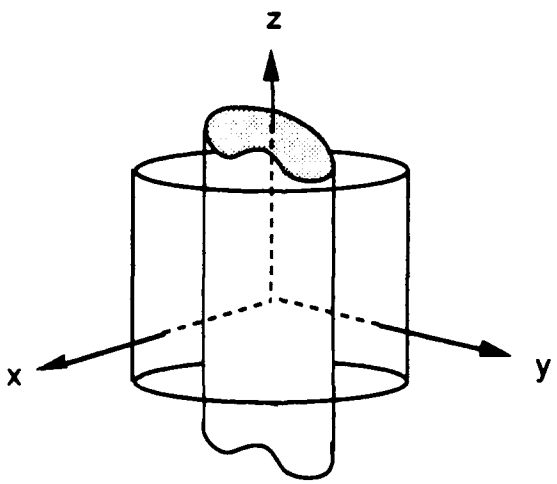

Fig 1.

We assume there is a plane wave of specified amplitude, polarization and angle of incidence given by the wave vector $\mathbf{k}_o$ propagating through the space and interacting with the scattering object. The fields outside the boundary of the cylinder may be written as the sum of the incident wave in terms of the components of the wave vector k_x, k_y, k_z and the wave frequency ω; and the scattered wave, which we shall express as a superposition of cylindrical waves of a known analytical form obtained from the solution of the wave equation incident on an ideal cylinder. The amplitude of this scattered wave is unknown and it contains information on the geometry and material characteristics of the scattering object. In terms of the (r,ϕ) coordinate system, the incident field is represented by

$$\mathbf{E}^i = e^{-i(\mathbf{r}\cdot\mathbf{k}_o - \omega t)}\left(E^i_{\parallel}\,\mathbf{e}_z + E^i_{\perp}\,\mathbf{e}_\phi\right) \qquad (2.1)$$

where $E^i{}_{\parallel}$ and $E^i{}_{\perp}$ are the parallel and perpendicular components of the incident field, and $k_o = (\mu\varepsilon)^{1/2}\,\omega/c$ where ω is the frequency of the incident wave.

The scattered field at a point P in the region outside the matching interface, can be written as

$$\mathbf{E}^s(P) = e^{-i\omega t}\sum_{n=-\infty}^{\infty} A_n\,H_n^{(1)}(k_o r)\,e^{i n\phi} \qquad (2.2)$$

where $H_n^{(1)}(k_o r)$ is the cylindrical Hankel function of the first kind of order n and argument $k_o r$. The constants A_n are complex numbers that depend on the geometry and the material characteristics of the scattering object. In the far-zone, which is when the conditions $k_o r >> (k_o a)^2$ and $r >> \lambda_o$ are satisfied, the E-field can be approximated by a large

argument expansion for the Hankel function and its analytical form can be written as

$$E^s(P) = \sqrt{\frac{2}{\pi}} \frac{e^{i(k_o r - \pi/4)}}{\sqrt{k_o r}} T(\phi) \qquad (2.3)$$

where

$$T(\phi) = \sum_{n=-\infty}^{\infty} A_n e^{i n(\phi - \pi/2)} \qquad (2.4)$$

The scattering cross section per unit length can be obtained as

$$\sigma(\phi) = \frac{4}{k_0} | T(\phi) |^2 \qquad (2.5)$$

The problem is now reduced to solving the wave equation inside the cylindrical boundary of radius r_o, and matching the solution (with a scaling factor) to the sum of the incident plane wave, (2.1), and the scattered cylindrical wave, (2.2), at the fictitious cylindrical surface where there is no source.

In the more general case, we can model the scattering object as a set of nested sharp interfaces across which the properties of the media changes discontinuously. A natural set of coordinates is one that conforms to this set of nested interfaces. Each surface is represented by setting one of the coordinates as a constant. We first identify the boundaries of the sharp interfaces of abruptly changing properties in the scattered object and assume that the material properties between the sharp interfaces is inhomogeneous and anisotropic but varies in a continuous manner. We define η as a coordinate function which is constant on each of the

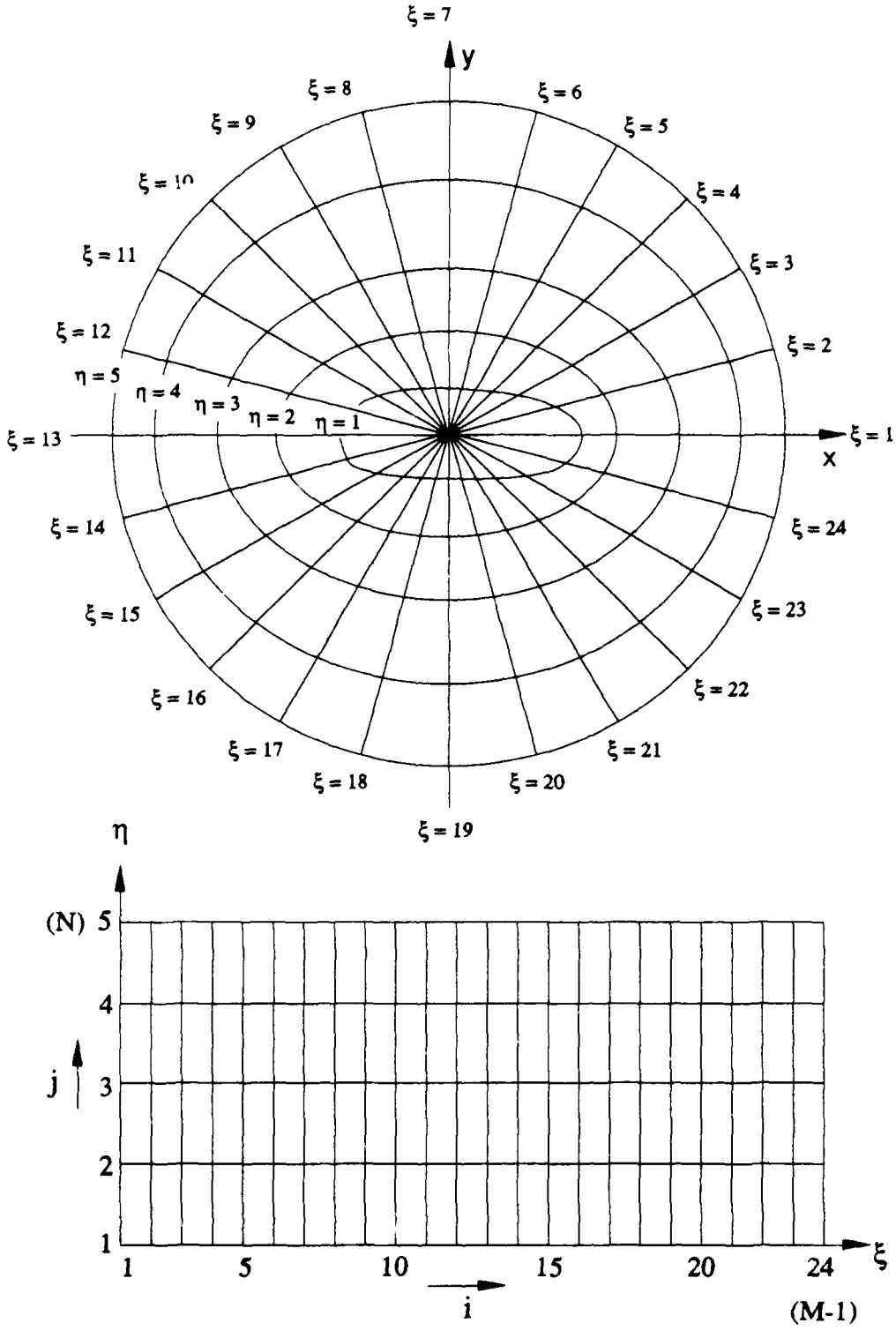

Fig. 2 Transformation of Physical Plane into Natural Coordinates.

interfaces. A second coordinate function ξ is chosen to intersect the η surfaces on the interfaces, and $\xi = \phi$ on the cylindrical boundary. We require both η and ξ to satisfy Laplace's equation

$$\nabla^2 \eta = 0 \tag{2.6}$$

and

$$\nabla^2 \xi = 0 \tag{2.7}$$

subject to Dirichlet boundary conditions. In general, the generated coordinate system will be orthogonal only if we require

$$\frac{\partial \eta}{\partial \xi} = 0 \tag{2.8}$$

However, this requirement would not allow for arbitrary spacing of the natural coordinate lines around the boundary. In the general case when this condition is not satisfied, the coordinate system will not be orthogonal. The system of governing equations must then be transformed directly through implicit partial differentiation rather than by use of scale factors and differential operators as is possible with orthogonal curvilinear systems. However, the advantages of allowing for arbitrary spacing far outweighs the complications of the transformation procedure which is carried out analytically only once. Therefore, we shall use the more general non-orthogonal curvilinear coordinate system. An example of the natural coordinate system in the physical plane of an irregular object is shown in Fig. 2.

The effect of the transformation in this two dimensional case is to convert a doubly connected region bounded by two closed contours of arbitrary shape in the physical plane into a rectangular region in the transformed plane in which two

of the opposite boundaries are coincident in the physical plane. As has been noted, the transformation must be carried out by taking the partial derivatives according to the chain rule. In general, the resulting equation will be considerably more complicated than the original form. However, the boundary conditions are now specified along straight lines and the equations are to be solved in a simple rectangular system.

The next step is to represent the Maxwell equations in the natural coordinate system and determine the wave equation for either the electric or the magnetic fields in the interior of the fictitious cylinder. We will also base our formulation on the tensorial representation of the equations and vector fields, since all the information about the geometry of the system can be contained in the components of the metric tensor which simplifies the formulation of the problem and the numerical algorithms, as a consequence.

For our present purpose, we shall consider the simplified problem of a two dimensional scattering object that is a perfect conducting infinite cylinder of arbitrary cross sectional shape and solve for the wave equation in the multiply connected region bounded by the scattering object and the minimum cylinder that completely encapsulate this object.

The Maxwell equations in the source free space are:

$$\nabla \cdot \mathbf{E} = 0 \tag{2.9}$$

$$\nabla \times \mathbf{E} = -\frac{1}{c}\frac{\partial \mathbf{B}}{\partial t} \tag{2.10}$$

$$\nabla \cdot \mathbf{B} = 0 \tag{2.11}$$

$$\nabla \times \mathbf{B} = \frac{1}{c}\frac{\partial \mathbf{E}}{\partial t} \tag{2.12}$$

where $\mathbf{E} = \mathbf{E}^i + \mathbf{E}^s$, $\mathbf{E}^i$ and $\mathbf{E}^s$ are the incident and scattered component of the electric field respectively. The same notation stands also for the magnetic field in the region.

The boundary conditions at the surface of the perfect conducting scatter are given by

$$\mathbf{e_n} \cdot \mathbf{E} = 4\pi\, q_s \tag{2.13}$$

$$\mathbf{e_n} \times \mathbf{E} = 0 \tag{2.14}$$

$$\mathbf{e_n} \cdot \mathbf{B} = 0 \tag{2.15}$$

$$\mathbf{e_n} \times \mathbf{B} = \frac{4\pi}{c}\, \mathbf{J_s} \tag{2.16}$$

where $\mathbf{e_n}$ is the unit vector normal to the scatter surface, and directed outward, q_s is the surface charge density, and $\mathbf{J_s}$ is the surface current density. From eqs.(2.10) and (2.12), a wave equation for the electric field can be written as

$$\nabla \times \nabla \times \mathbf{E} = -\frac{1}{c^2}\frac{\partial^2 \mathbf{E}}{\partial t^2} \tag{2.17}$$

We shall represent this equation in terms of the natural coordinates by making use of the conformal transformation described in Appendix B. In order to simplify the analysis, and to be able to present bench mark cases, we will assume that the E-field of the incident plane wave is linearly polarized in the direction parallel to an infinitely long circular cylinder which is a perfect conductor. Therefore, the scattered electric field will also be polarized parallel to the cylinder axis. The wave equation given by (2.17) becomes a scalar equation for E^s, which is the scattering field in the physical domain (x,y), and it can be written as

$$\nabla^2 E^s_{in} + k_0^2\, E^s_{in} = 0 \tag{2.18}$$

with the boundary conditions

$$[\, E^s_{in}(x,y)\,]_{body} = -[\, E^i(x,y)\,]_{body} \tag{2.19}$$

$$[\, E^s_{in}(x,y)\,]_{R_0} = [\, E^s_{out}(\phi,r)\,]_{R_0} \tag{2.20}$$

where E_{out} is the scattering field outside the matching boundary, of radius R_0, and E^i is the incident plane wave. We also require that the normal derivative of E_{in} be continuous at R_0, that is,

$$\left[\frac{\partial E^s_{in}}{\partial n}\right]_{R_0} = \left[\frac{\partial E^s_{out}}{\partial n}\right]_{R_0} \tag{2.21}$$

When transformed to the natural coordinate system, by making use of Eq.B.13 in appendix B, the above wave equation (2.18) becomes

$$\alpha E_{\zeta\zeta} - 2\beta E_{\zeta\eta} + \gamma E_{\eta\eta} + J^2 k_0^2 E = 0 \tag{2.22}$$

where E is a function of (ξ, η), and $E_{\xi\xi}$, $E_{\xi\eta}$ and $E_{\eta\eta}$ are its partial derivatives. The metric elements and the Jacobian, J, of the transformation are calculated in Appendix B and can be written as

$$\alpha = x_\eta^2 + y_\eta^2 \tag{2.23}$$

$$\beta = x_\xi x_\eta + y_\xi y_\eta \tag{2.24}$$

$$\gamma = x_\xi^2 + y_\xi^2 \tag{2.25}$$

$$J = x_\xi y_\eta - x_\eta y_\xi \tag{2.26}$$

The transformed boundary conditions are

$$[\, E^s_{in}(\xi,\eta)\,]_{\eta_1} = [\, E^i(\xi,\eta)\,]_{\eta_1} \tag{2.27}$$

$$[\, E^s_{in}(\zeta,\eta)\,]_{\eta_0} = [\, E^s_{out}(\phi,r)\,]_{R_0} \tag{2.28}$$

$$\left[\frac{\partial E^s_{in}(\xi,\eta)}{\partial \eta}\right]_{\eta_0} = \left[\frac{\partial E^s_{out}(\phi,r)}{\partial r}\right]_{r=R_0} \tag{2.29}$$

where $\xi \rightarrow \phi$ when $\eta \rightarrow \eta_0$. The coefficients α, β, γ and the Jacobian are calculated during the generation of the natural coordinate system.

After the mesh is generated, the Helmholtz equation in natural coordinates, (2.22), is to be solved by using finite difference techniqes. Since the factors α, β, γ and J are function of the two coordinates ξ and η, the Helmholtz equation has variable coefficients. However, this presents no difficulty in the numerical solution.

The Helmholtz equation can be approximated as a set of linear algebraic equations by the use of finite differences. The matrix resulting from the finite difference equations is sparse and well conditioned. As a result, standard sparse matrix subroutines that perform Gaussian elimination can be used to solve the set of linear equations. The use of a sparse matrix solver makes the overall method very efficient with respect to computational resources. Test cases demonstrating the accuracy of the solution are presented in the following chapter.

III. EXAMPLES OF BENCH MARK CALCULATIONS

To carry out the cross section calculations based on our approach, we had to develop two computational modules. The first module is for generation of the natural coordinate system in the region between the scattering object and the fictitious interface and transform of the wave equation in this region into the natural coordinate system. The formulation for the determination of the natural coordinate system is described in detail in Appendix A. The algorithm for the transformation of the wave equation into the natural coordinate system is described in Appendix B. The numerical technique for the solution of the wave equation in the natural coordinate system and matching of the solution at the fictitious interface to the series solution outside the interface is described in Appendix C. In this section, we present examples of calculated results and benchmark cases to illustrate the application of the code to calculate the radar cross section of two dimensional objects of arbitrary shape.

A. Generation of the Natural Coordinate System

The objective for defining a natural coordinate system is to transform the governing equations from doubly connected region R bounded by contours (surfaces for the fully three dimensional case) of arbitrary shape into a rectangular region R'. The effect is illustrated in Fig. 3 that relates the region between a scattering object and an enclosing circle in the (r,θ) or (x,y) physical space to a rectangle in (η,ξ) natural coordinate space. The natural coordinates (η,ξ) are obtained from solutions of Laplace's equations for η and ξ with Dirichlet boundary conditions: η = constant = η_1 on C_1 , η = constant = η_2 on C_2; $\xi(x,y)$ is a multiple valued solution with a branch of $\xi(x,y)$ specified (but not constant) on C_1 and C_2 . The curve C_1 on the physical plane transforms to the

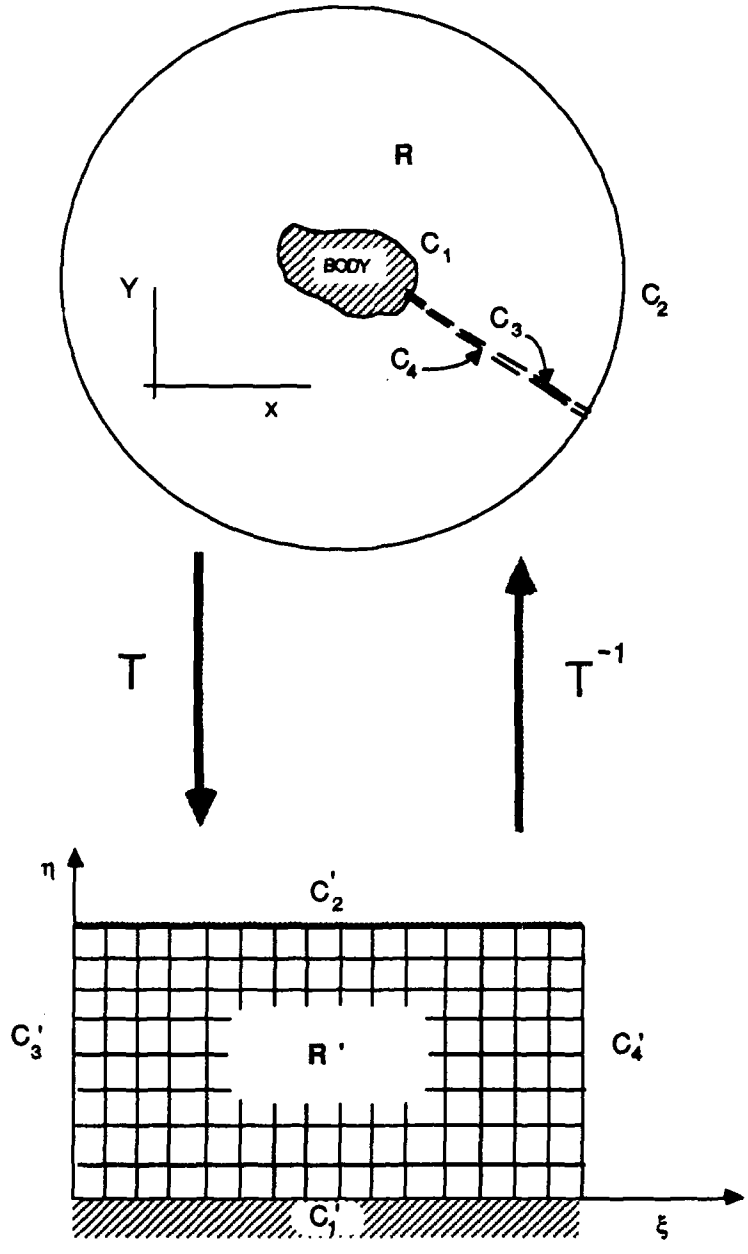

Fig. 3 Mapping of the coordinate transformation

lower boundary, C_1', of the transformed plane. Similarly, C_2 transforms to C_2', etc. The right and left boundaries of the rectangular transformed plane, C_3' and C_4', are coincident in the physical plane. The curve which transforms to these boundaries connects C_1 and C_2 and determines a branch cut for the multiple valued function $\xi(x,y)$. Thus the functions and all derivatives are continuous across this cut.

The natural coordinate system so generated has a constant η-line coincident with each boundary in the physical plane. The ξ-line may be spaced in any manner desired around the boundaries by specification of the ξ boundary conditions, or equivalently by specification of (x,y) at the equi-spaced ξ-points on the η_1 and η_2 lines of the transformed plane. Control of the spacing of the η-lines may be exercised by varying the elliptic system of which η and ξ are solutions.

To test the module, we have carried out the calculation for the generation of the natural coordinate grids for a number of two dimensional objects with geometric cross sections of circles, ellipses, rectangles and crosses. To speed convergence, we have found founding of sharp corners as shown to be helpful but not necessary. Examples for each of the four cases are shown in Fig. 4, 5, 6 and 7, respectively. All computations were carried out on an IBM 3090. Using the algorithm, convergence to less than 1% deviation is achieved in only a few iterations for the elliptic case as shown in Fig. 8a and 8b where we have plotted the normalized changes in the x and y coordinates of the grid for the natural coordinate system as a function of the number of iterations. Convergence to 0.2% is realized typically in 30 iterations and the accuracy continues to improve with further iterations. Similar behavior are found for the other cases where we have carried out bench mark calculations to determine the number of iterations and computer processor unit (CPU) time in seconds on the IBM 3090 as a function of

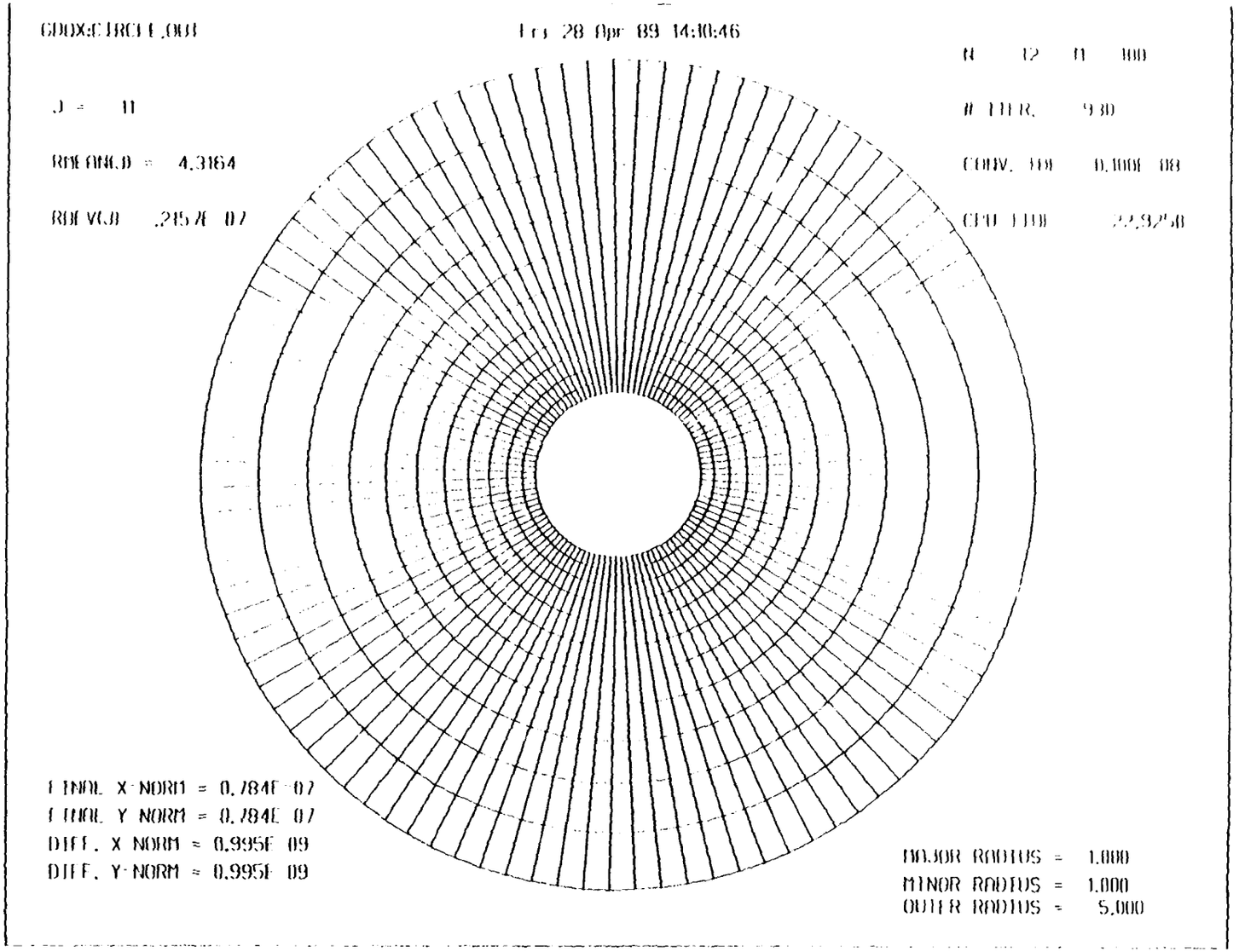

Fig. 4 Natural coordinate for circular object

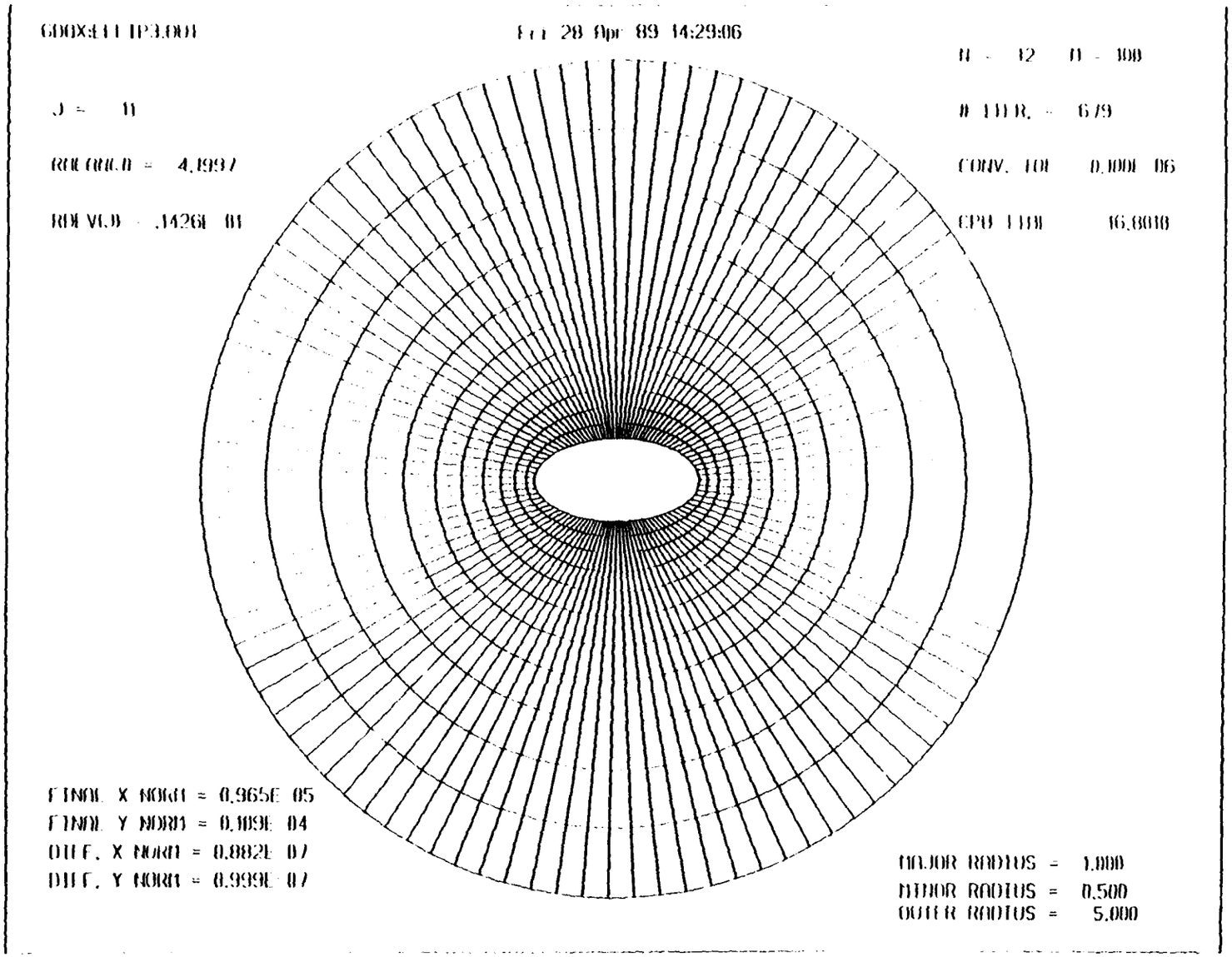

Fig. 5 Natural coordinates for elliptical object

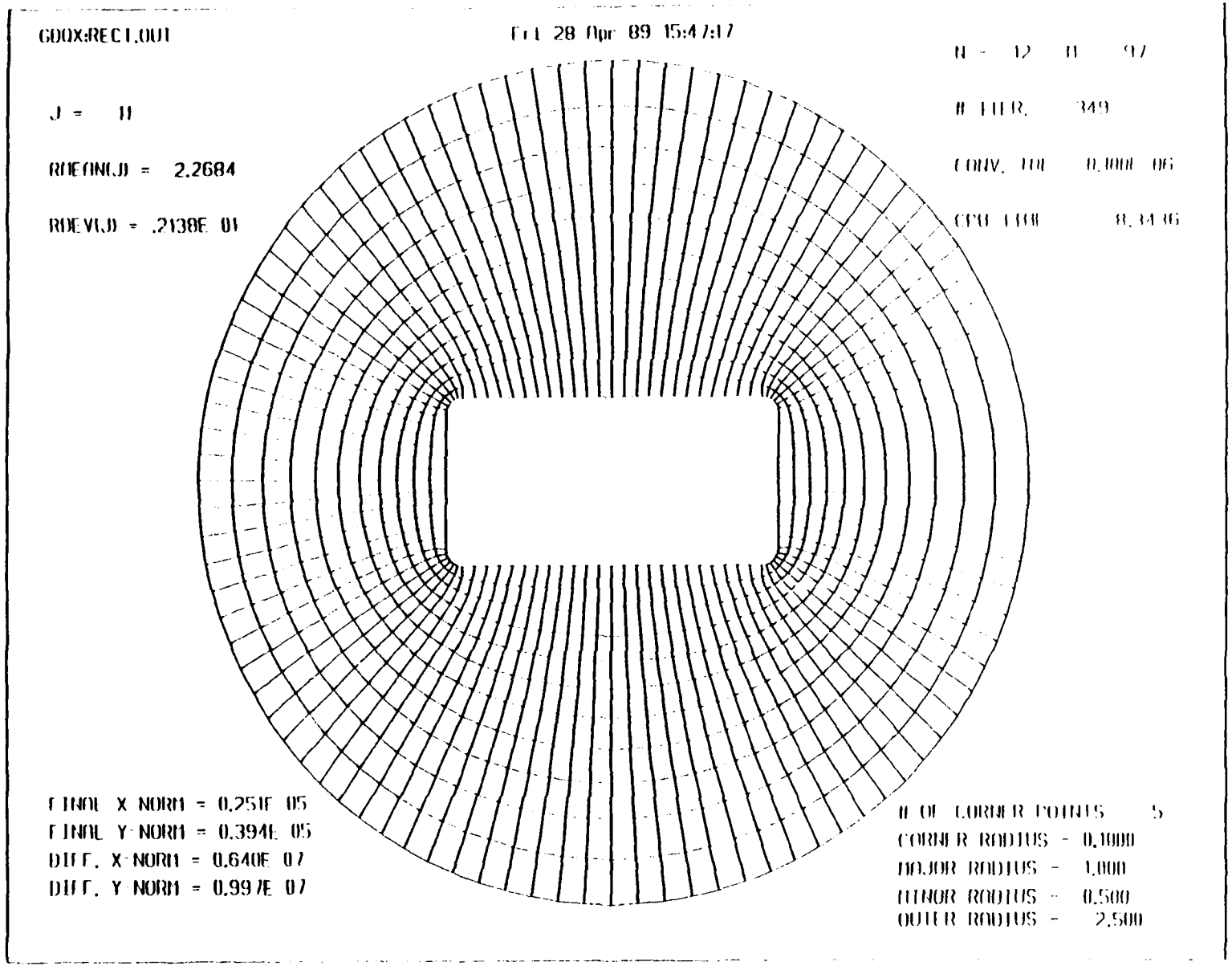

Fig. 6 Natural coordinate system for rectangular object

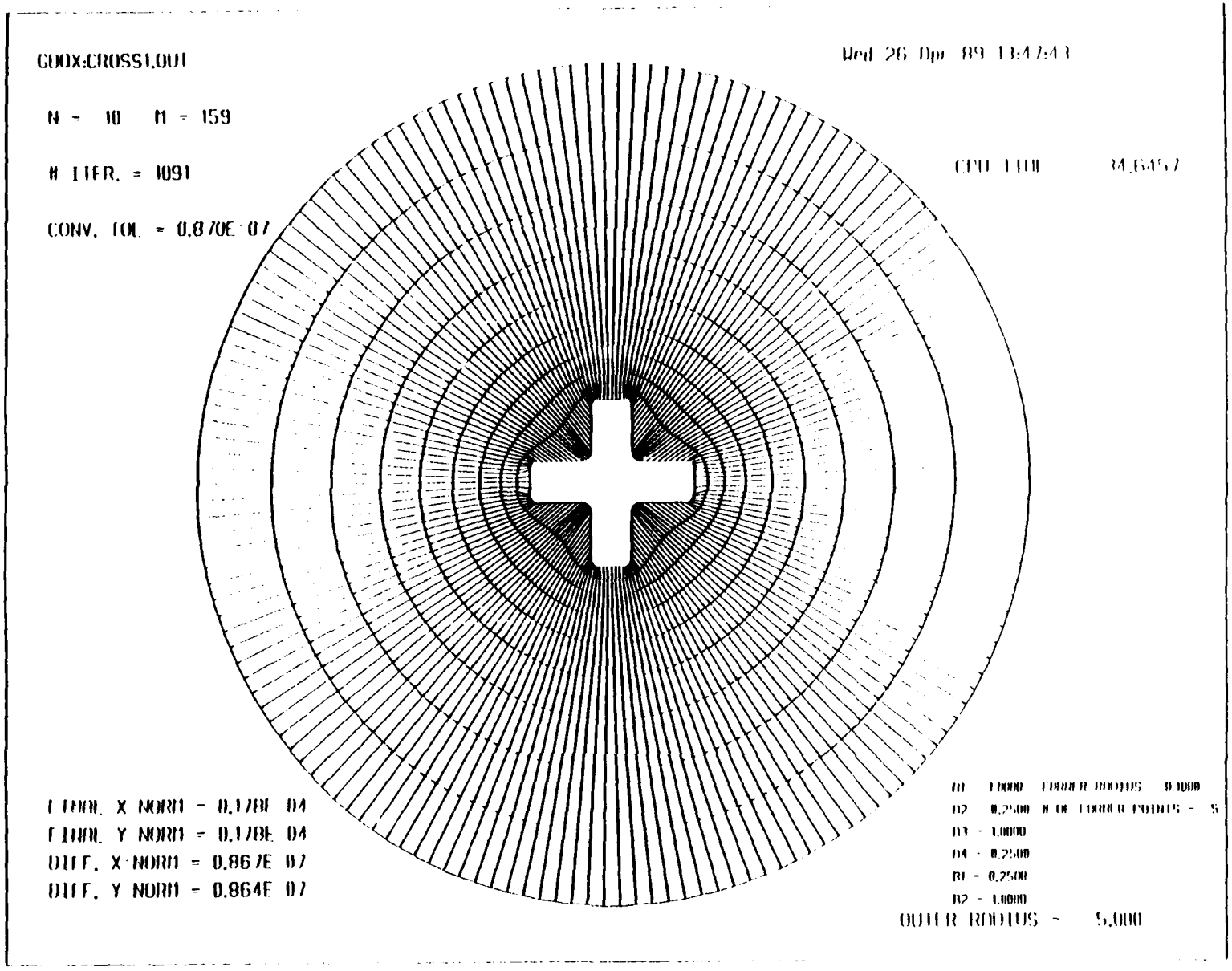

Fig. 7 Natural coordinate system for a cross

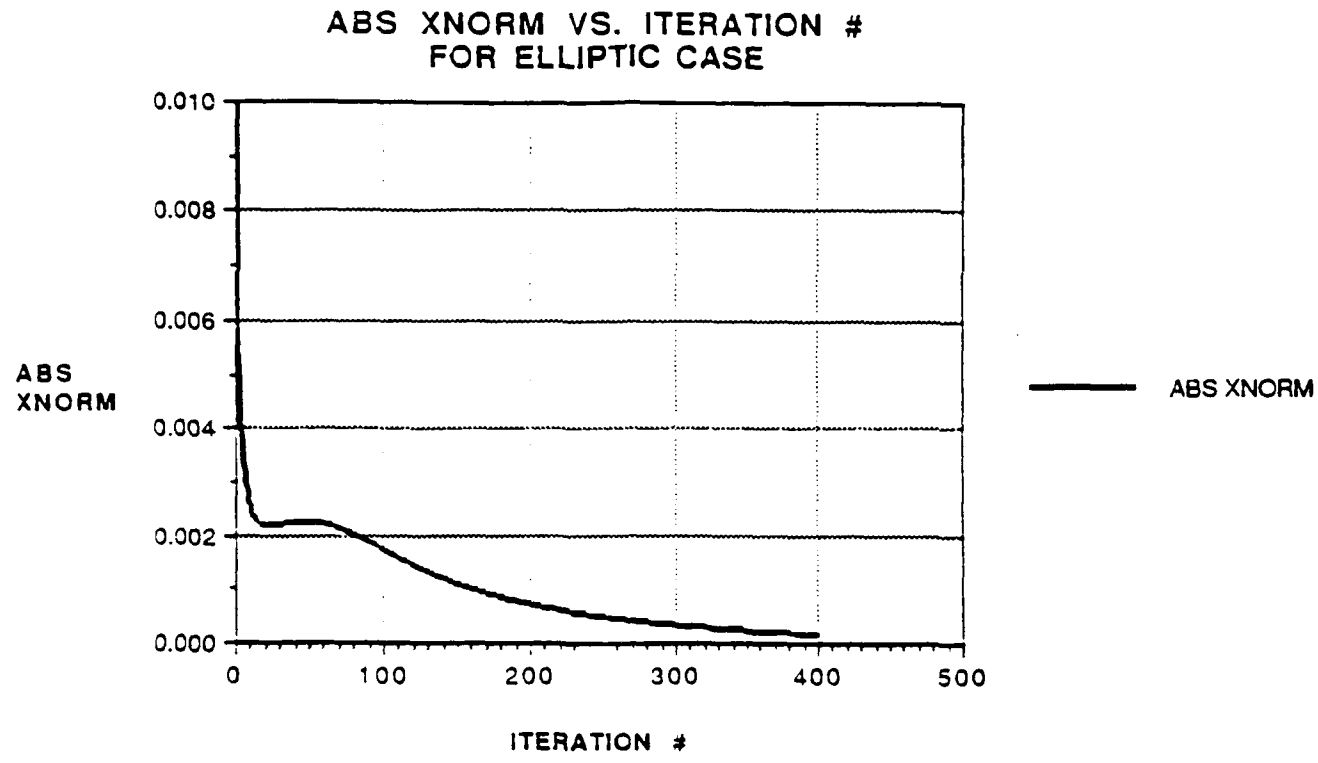

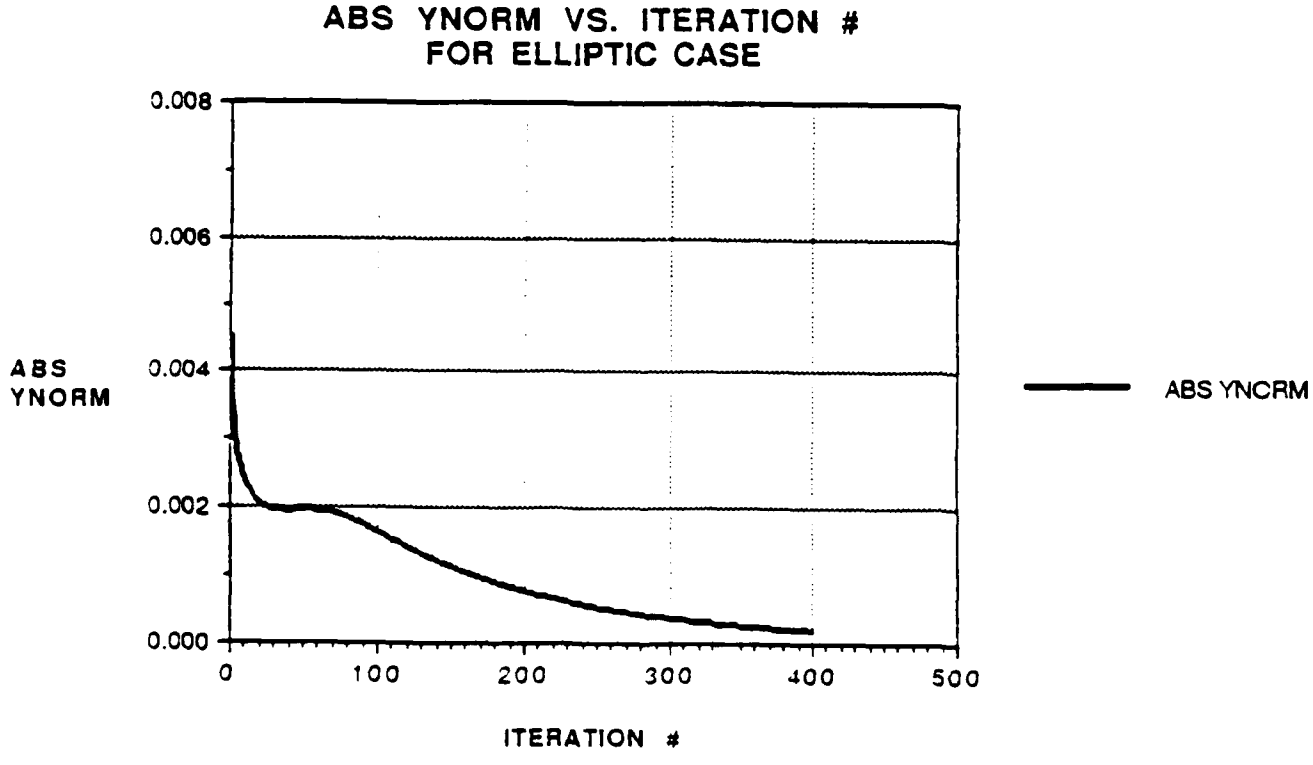

Fig. 8 Convergence of the x and y coordinates of the natural coordinate system

convergence tolerance specified. The results are shown in Fig. 9a, 9b and 9c for the case of the ellipse, cross and rectangle, respectively. In all cases, the CPU time is less than a few seconds for convergence tolerance of less than one part per million. At this point in the development of the code, we have made no effort to optimize the code and even so, the computational requirement for the generation of the natural coordinate system is quite insignificant.

B. Verification of the Helmholtz Solver

Making use of the natural coordinate system, the next task is to transform the governing equations into the natural coordinate system and solve the system of equations numerically subject to the transformed boundary conditions. To test the algorithm, we carried out a benchmark calculation of a cylindrical stationary wave subject to simple boundary conditions for which an exact analytical solution is available for comparison.

The governing equation is the Helmholtz equation which has the form

$$\nabla^2 E_{ex} + k^2 E_{ex} = 0 \tag{3.1}$$

In cylindrical coordinates this becomes

$$\frac{1}{r}\frac{\partial}{\partial r}\left(r\frac{\partial E_{ex}}{\partial r}\right) + \frac{1}{r^2}\frac{\partial^2 E_{ex}}{\partial \phi^2} + k^2 E_{ex} = 0 \tag{3.2}$$

Assuming E_{ex} has the form

$$E_{ex} = E(r)\cos\phi \tag{3.3}$$

The solution of the equation is

$$E_{ex} = \{AJ_1(kr) + BY_1(kr)\}\cos\phi \tag{3.4}$$

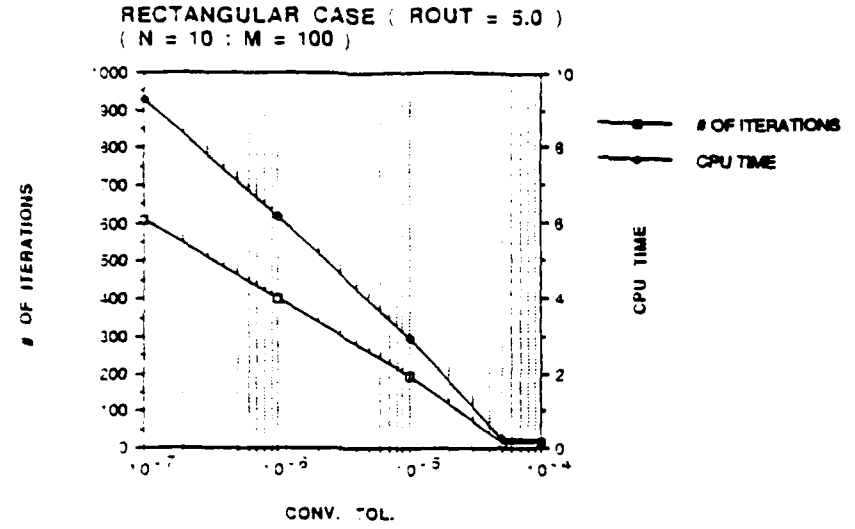

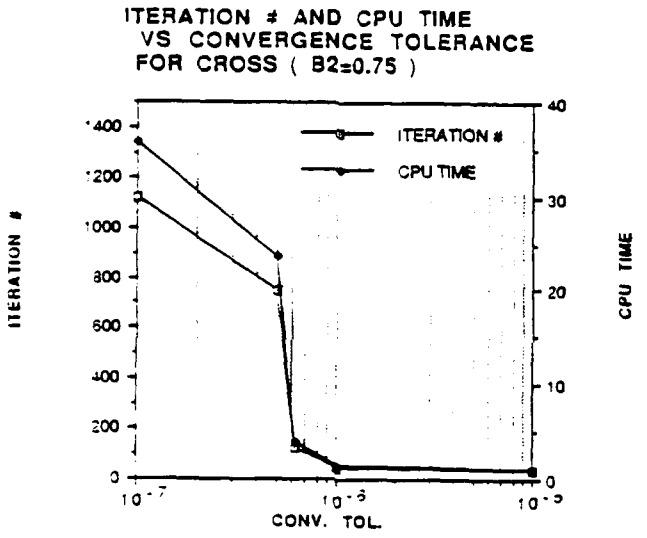

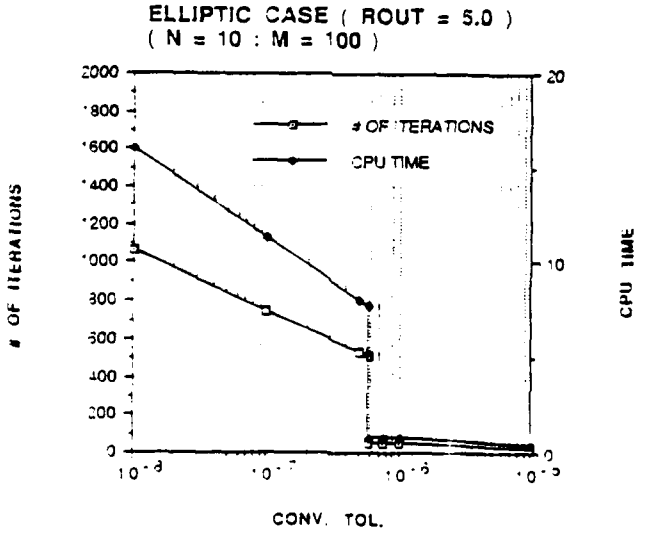

Fig. 9 Plot of number of interaction for specified convergence tolerence for (a) retangular case (b) a cross and (c) an ellipse

where $J_1(kr)$ and $Y_1(kr)$ are Bessel functions of the first and second kind respectively. Using the boundary conditions

$$E_{ex}|_{r=1} = 0 \tag{3.5}$$

$$E_{ex}|_{r=r_0} = \cos\phi \tag{3.6}$$

implies

$$A = \frac{-Y_1(k)}{J_1(k)Y_1(kr_0) - J_1(kr_0)Y_1(k)} \tag{3.7}$$

and

$$B = \frac{J_1(k)}{J_1(k)Y_1(kr_0) - J_1(kr_0)Y_1(k)} \tag{3.8}$$

which gives the exact solution.

The numerical solution is obtained by transforming the Helmholtz equation into the natural coordinate system. The resulting equation in the (η,ξ) space has the form

$$\alpha E_{\xi\xi} - 2\beta E_{\xi\eta} + \gamma E_{\eta\eta} + k^2 J^2 E = 0 \tag{3.9}$$

with the boundary conditions

$$E(\xi,\eta)|_{\eta=1} = 0 \quad \text{and} \quad E(\xi,\eta)|_{\eta_0} = \cos\xi \tag{3.10}$$

The equations are solved numerically and the results are compared with the exact analytical solution as shown in Fig. 10a, 10b and 10c in which we compared the solutions along a radial cut at 45-degree angle for three cases by taking 20, 40 and 60 radial grids. The points represented by the black diamonds are the numerical results while the open squares represent the exact analytical values calculated at the corresponding grid position. The improved agreement of the

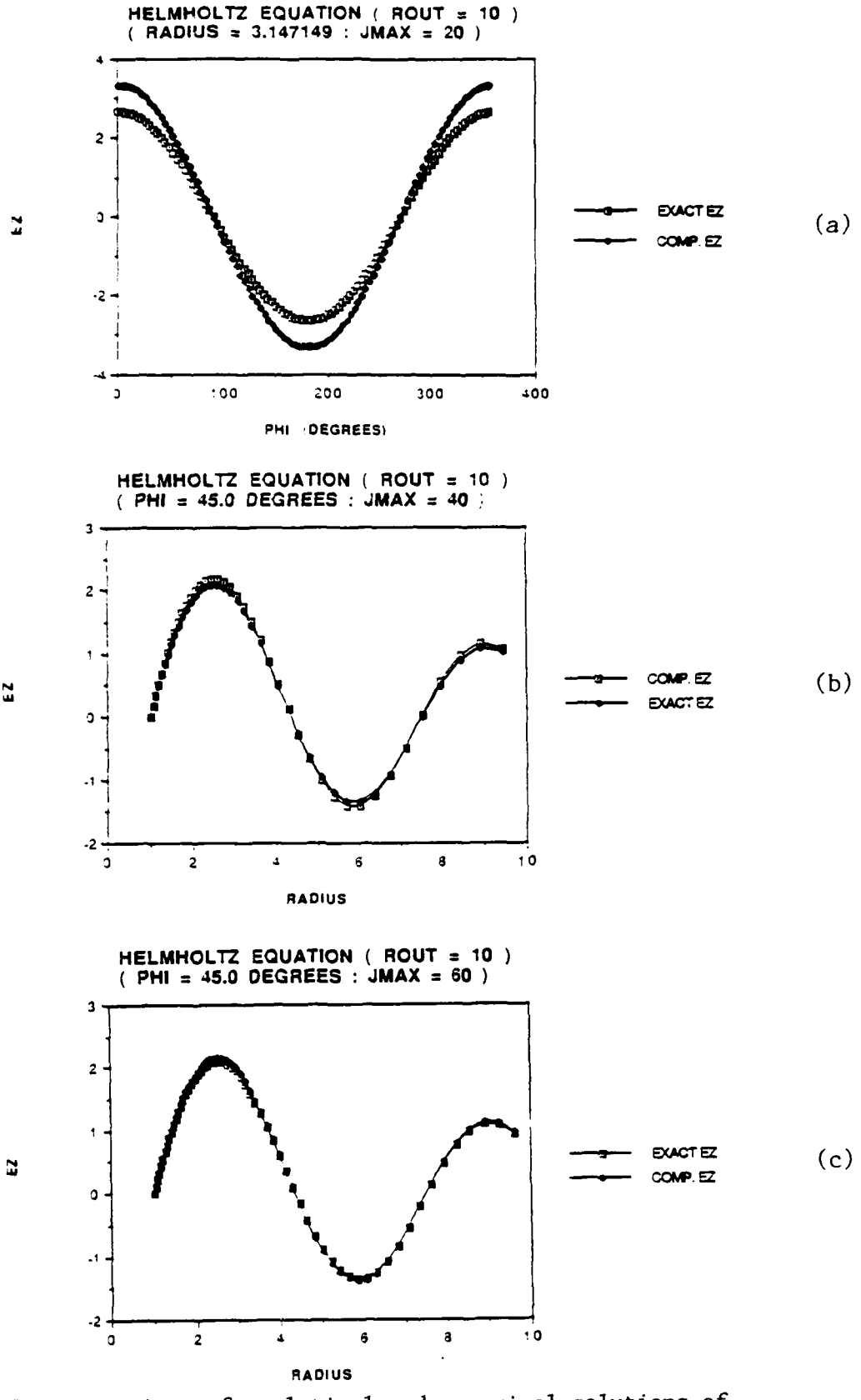

Fig. 10 Comparison of analytical and numerical solutions of Helmholtz equation at a constant radius for (a) 20, (b) 90, and (c) 60 radical grids

numerical solution with the analytical solution with refinement to the radial grid is readily apparent. Excellent agreement is realized by taking 60 mesh points. The agreement between the solutions as a function of the angle at a constant radius for the three cases are shown in Figs. 11a, 11b and 11c. It can be seen that the trend is similar.

Based on these results, we concluded that by chosing a fine enough mesh, the numerical solver will match to the exact solution. This is due to the fact that the (x,y) points generated have an error of $O(h^2)$ where h = the step size in the radial direction. So as the number of η-lines is increased h will decrease and the computed solution will become a better approximation to the exact solution. When a mesh of ξ_{max}= 53 and η_{max} = 42 is used a mean difference between the exact solution and the computed solution normalized with respect to the exact solution of 4.5% while with a mesh of ξ_{max}= 53 and η_{max} = 62 the mean difference between the exact solution and the computed solution normalized with respect to the exact solution was found to be 2.6%. This implies that as the mesh is refined the computed solution is converging to the exact solution.

It was also observed that the number of ξ-lines does not have as great an effect on convergence as the number of η-lines. In going from a mesh of ξ_{max} = 97 and η_{max} = 21 to a mesh of ξ_{max} = 53 and η_{max} = 42 the doubling of the number of η-lines overcomes any decrease in convergence from decreasing the number of ξ-lines.

C. Results of Cross Section Calculations

To establish the validity of the code, we compare the results of the numerical calculations to the analytical results for scattering from a perfect conducting infinite cylinder of circular geometric cross section. An analytical

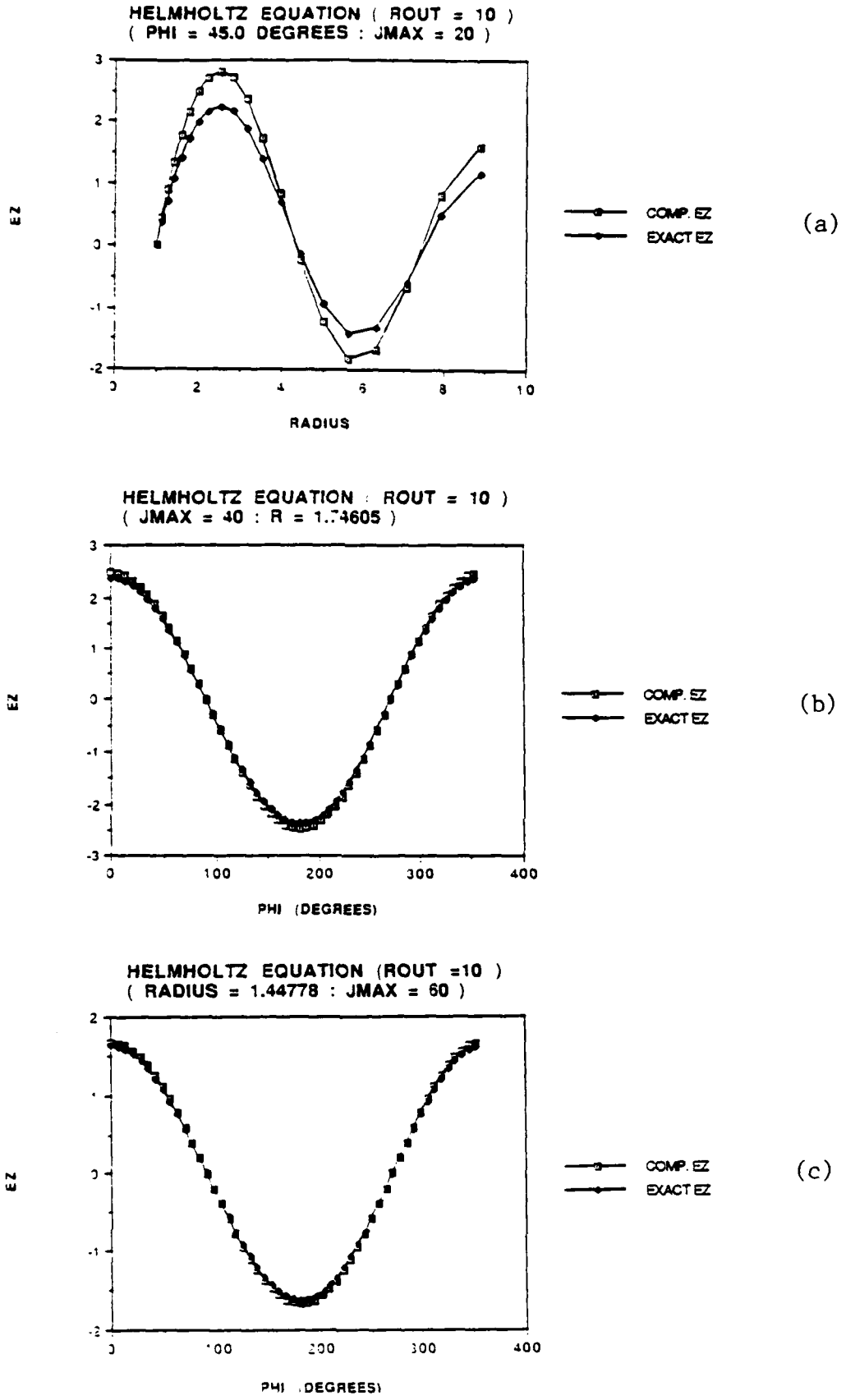

Fig. 11 Comparison of analytical and numerical solutions of Helmholtz equation at a constant radius for (a) 20, (b) 90, and (c) 60 radical grids

solution for the case when the incident electric field is linearly polarized (parallel to the axis of the cylinder) is given in Appendix D, which is of the form

$$E^s = \sum_{n=0}^{\infty} (-i)^n \varepsilon_n A_n H_n^{(1)}(k_0 r) \cos(n\phi) \qquad (3.11)$$

$$\text{with} \quad \varepsilon_n = \begin{cases} 1 \text{ for } n = 0 \\ 2 \text{ for } n = 1,2,3,\ldots \end{cases}$$

where A_n is the coefficient of the n^{th} harmonic in the series representation of the analytical solution. For waves scattered by an infinite cylinder, the magnitude of A_n as a function of n for the first five harmonics are shown in Fig. 12a. It can be seen that for low wave frequencies (or ka values) the magnitude of A_n falls off very rapidly with increasing n such that the contributions from high order modes will be negligible. Fig. 12b shows that for higher frequencies the contributions from high order modes is very significant. In matching the interior solution to the external analytical solution at the boundary, we need to evaluate many high order terms for higher frequency incident waves.

The total electric field as a function of the angle around the scattering object for waves incident along $\phi_0 = 0$ is shown plotted in Fig. 13. The corresponding differential scattering cross section as a function of the scattered angle is shown in Fig. 14 for the case k = 1. In general, for high wave numbers, the cross section is maximum in the forward direction. The forward ($\phi = \pi$) and backward ($\phi = 0$) scattering cross section as a function of the wave number is shown in Figs. 15 and 16, respectively. These results calculated from the analytical expression provide a reference for evaluating the accuracy of our numerical solution.

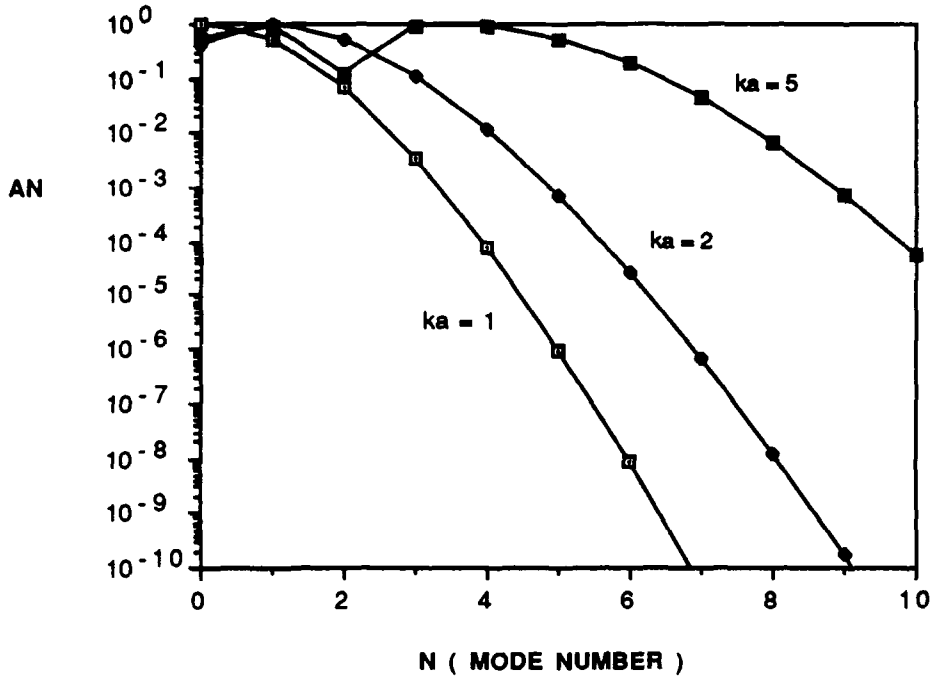

Fig. 12A

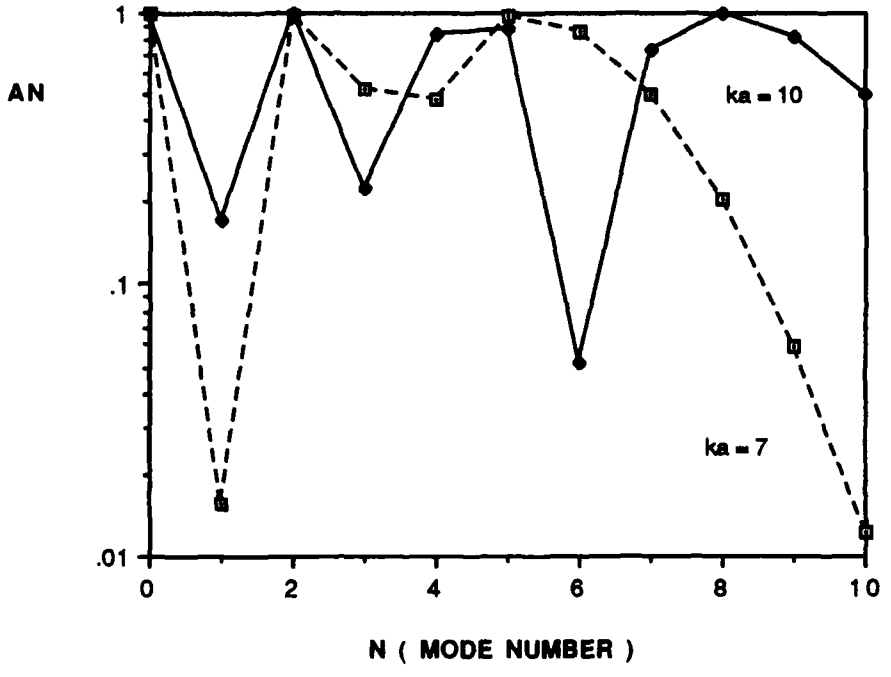

Fig. 12B

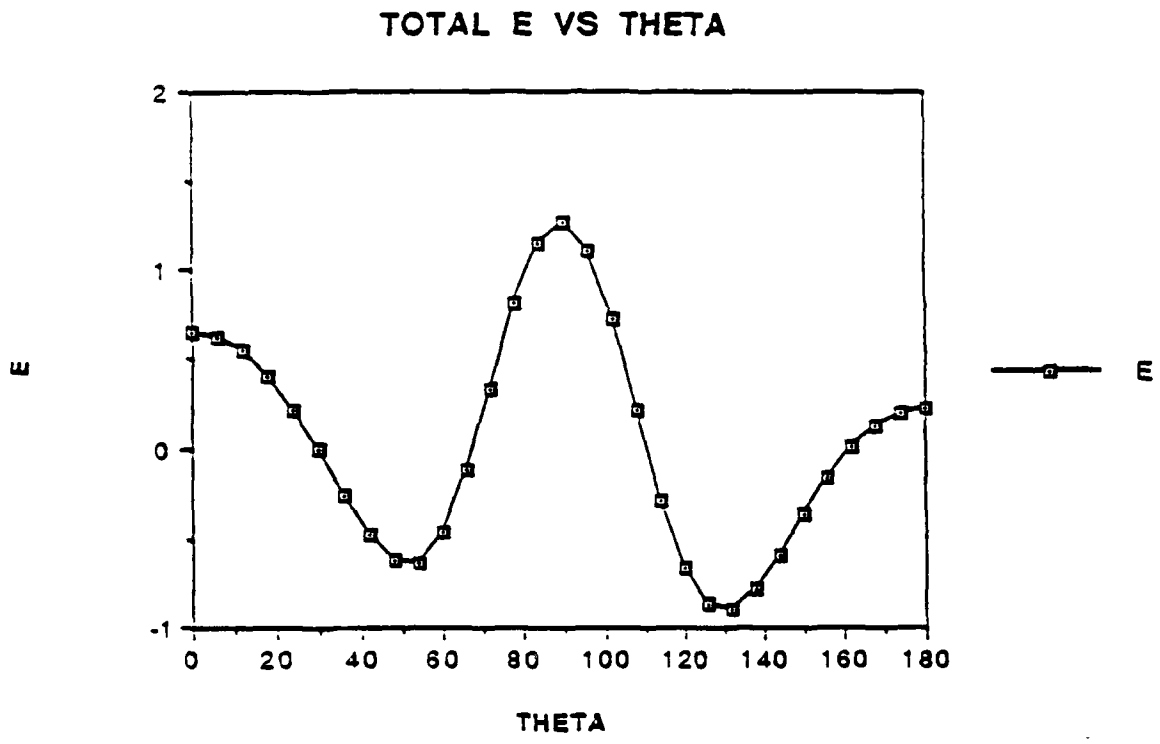

Fig. 13 Analytical solution of the total electric field as a function of scattered angle

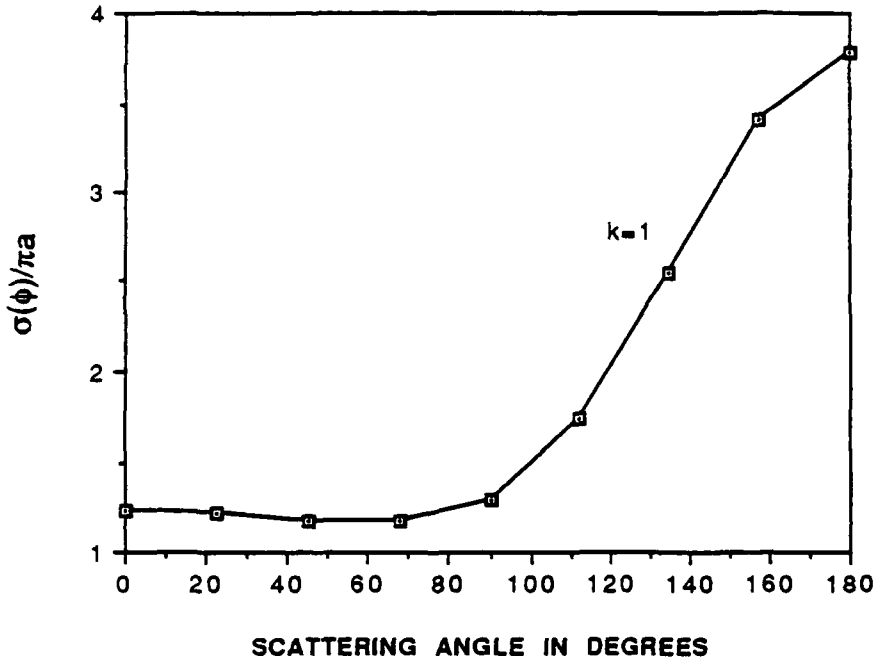

Fig. 14 Differential scattering cross section for k=1

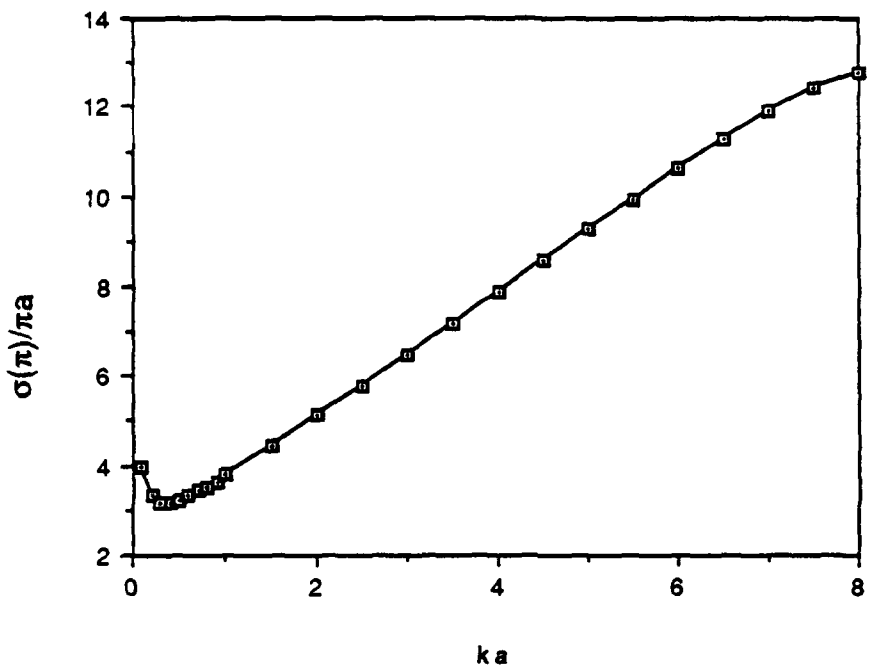

Fig. 15 Forward scattering cross section as a function of wave number

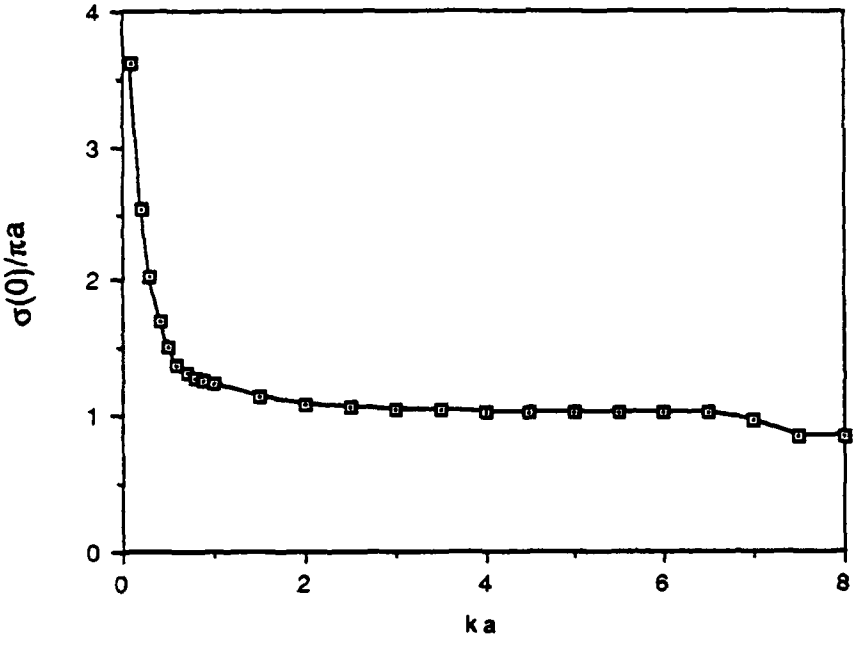

Fig. 16 Backscattering cross section as a function of wave number

The differential scattering cross section for the infinite cylinder calculated with the code was used as a bench mark. The results for the case of an incident wave with wave number k = 1 is shown in Fig. 17 in which the differential scattering cross section as a function of the scattered angle is given by the curve on top and the natural coordinate grid used for the calculation is shown at the bottom. The results calculated with the code is compared with the cross section obtained from the analytical solution as shown in Fig. 18. The absolute value of the normalized cross section are compared in the top figure and their differences as a function of the scattered angle are plotted in the bottom figure. It can be seen that the agreement is very good and the deviation is less than 1% at all scattered angles.

To further verify the accuracy of the numerical procedure, we evaluated the coefficient of the individual harmonics at the matching interface for comparison with the coefficients determined from the analytical solution. The results are shown in Fig. 19 for the case ka = 1. It is seen that the agreement is very good for the first five harmonics. Since the contributions of the high order harmonics is totally negligible in this case, it is reasonable to expect the high degree of agreement between the two results.

To exercise the code, we calculated the differential scattering cross sections for a variety of shapes by systematically varying the wave number, the angle of incidence and the number of modes included. In general, for ka < 5, we found that higher order terms has negligible effect on the solution as was to be expected. The cases calculated are summarized in Table 1. The results are shown in Figs. 20 through 30 and a variety of trends can be observed, some are intuitively obvious and many are quite interesting.

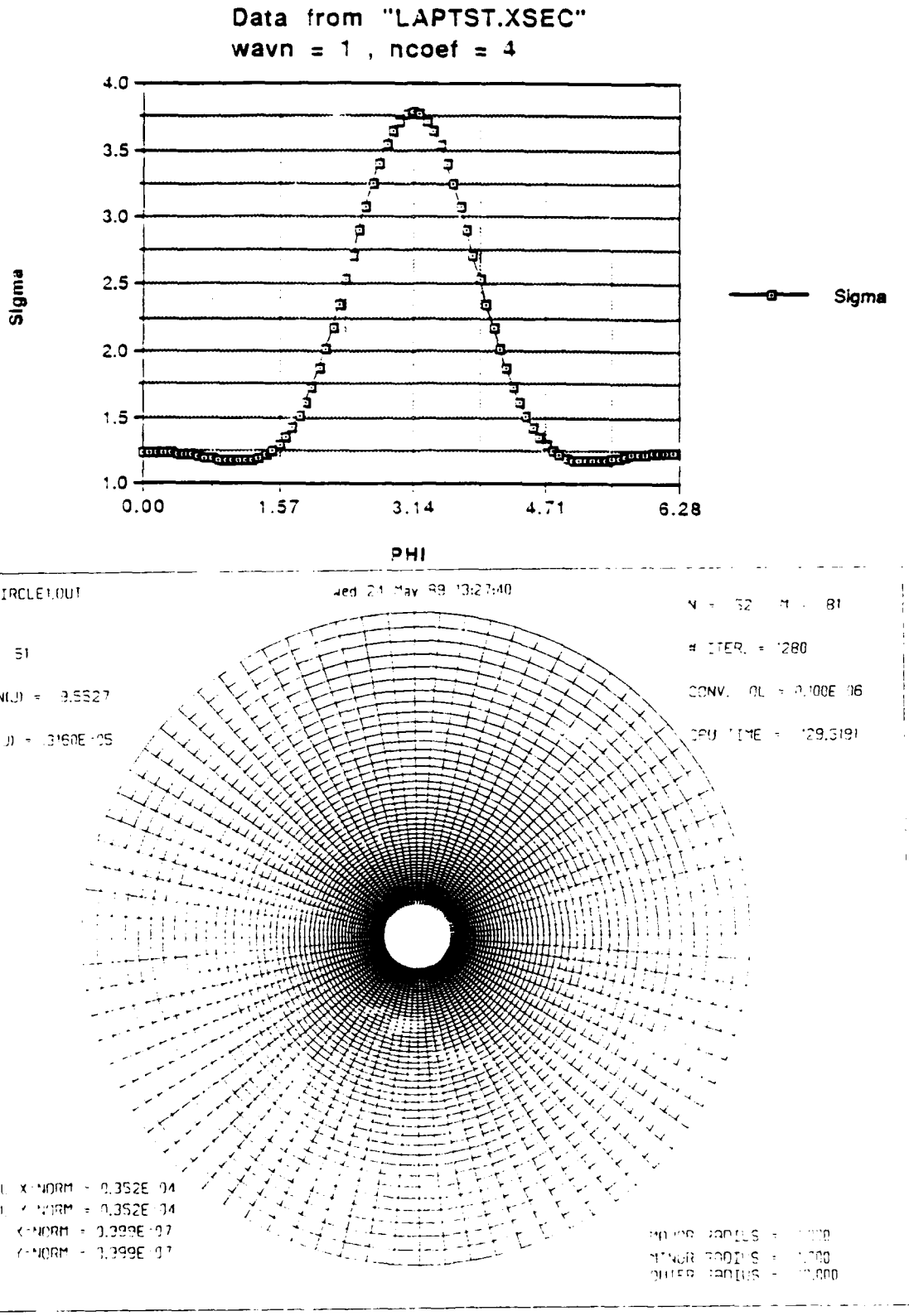

Fig. 17 Differential cross section of an infinite cylinder for ka=1 .

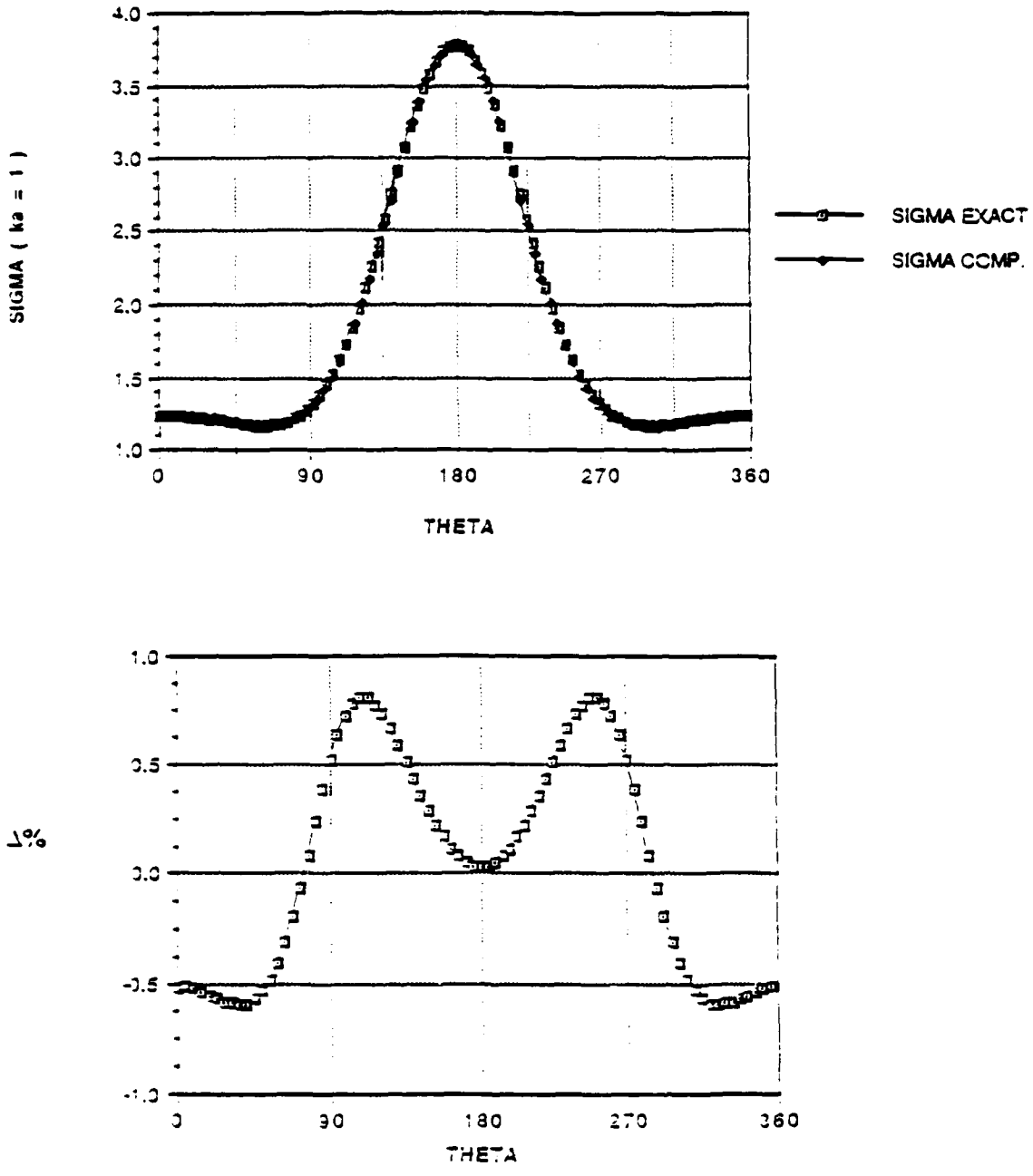

Fig. 18 Comparison of the differential cross section calculated analytically and numerically.

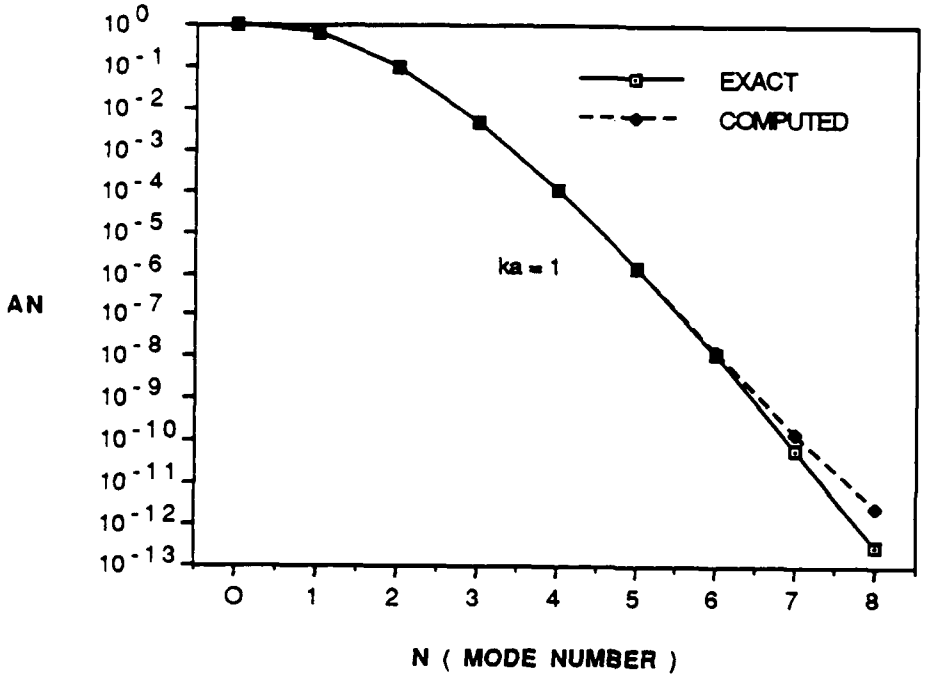

Fig. 19 Comparison of the harmonic coefficient for the analytical and numerical solutions

Table 1. Summary of Cross Section Calculation.

Fig. No.	Shape	Wave Number	No. of Modes	Angle of Incidence
20	Ellipse	0.5	6	0°
21	Ellipse	1.0	6	0°
22	Ellipse	3.0	6	0°
23	Ellipse	5.0	6	0°
24	Short Rectangle	1.0	4	0°
25	Long Rectangle	1.0	4	0°
26	Short Arm Cross	1.0	4	0°
27	Short Arm Cross	1.0	4	45°
28	Short Arm Cross	1.0	4	90°
29	Short Arm Cross	1.0	4	Varied
30	Long Arm	1.0	4	0°

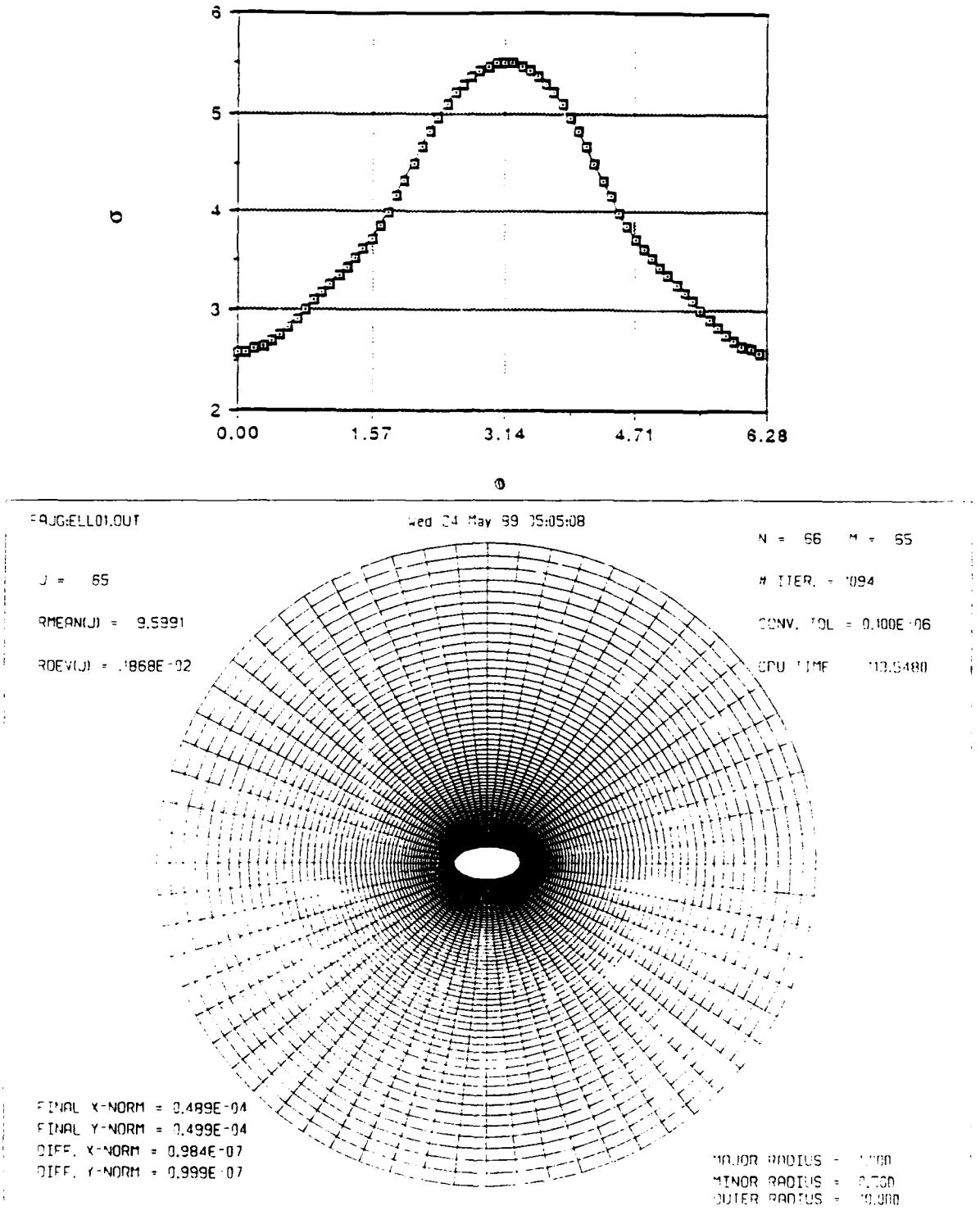

Fig. 20 Top figures cross section of a 1x2 elliptic cylinder for ka=0.5 and n=6 modes. Bottom figure shows the grid.

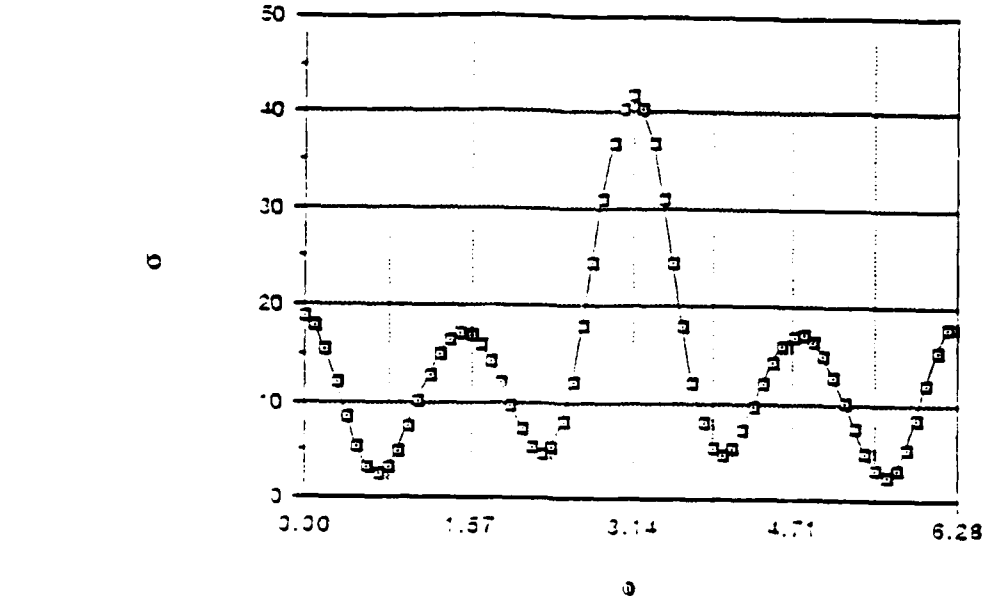

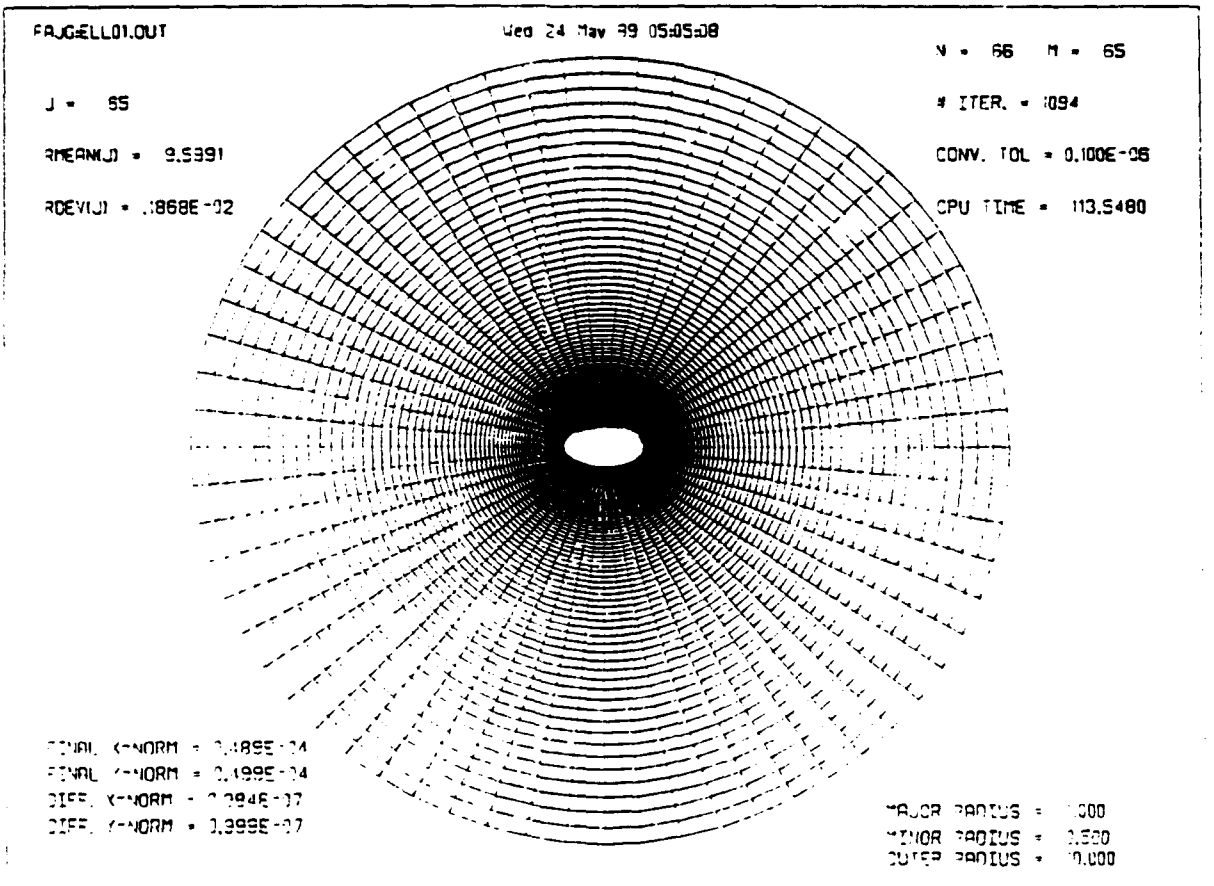

Fig. 21 Cross section of a 1x2 elliptic cylinder for ka=1 and n=6 modes.

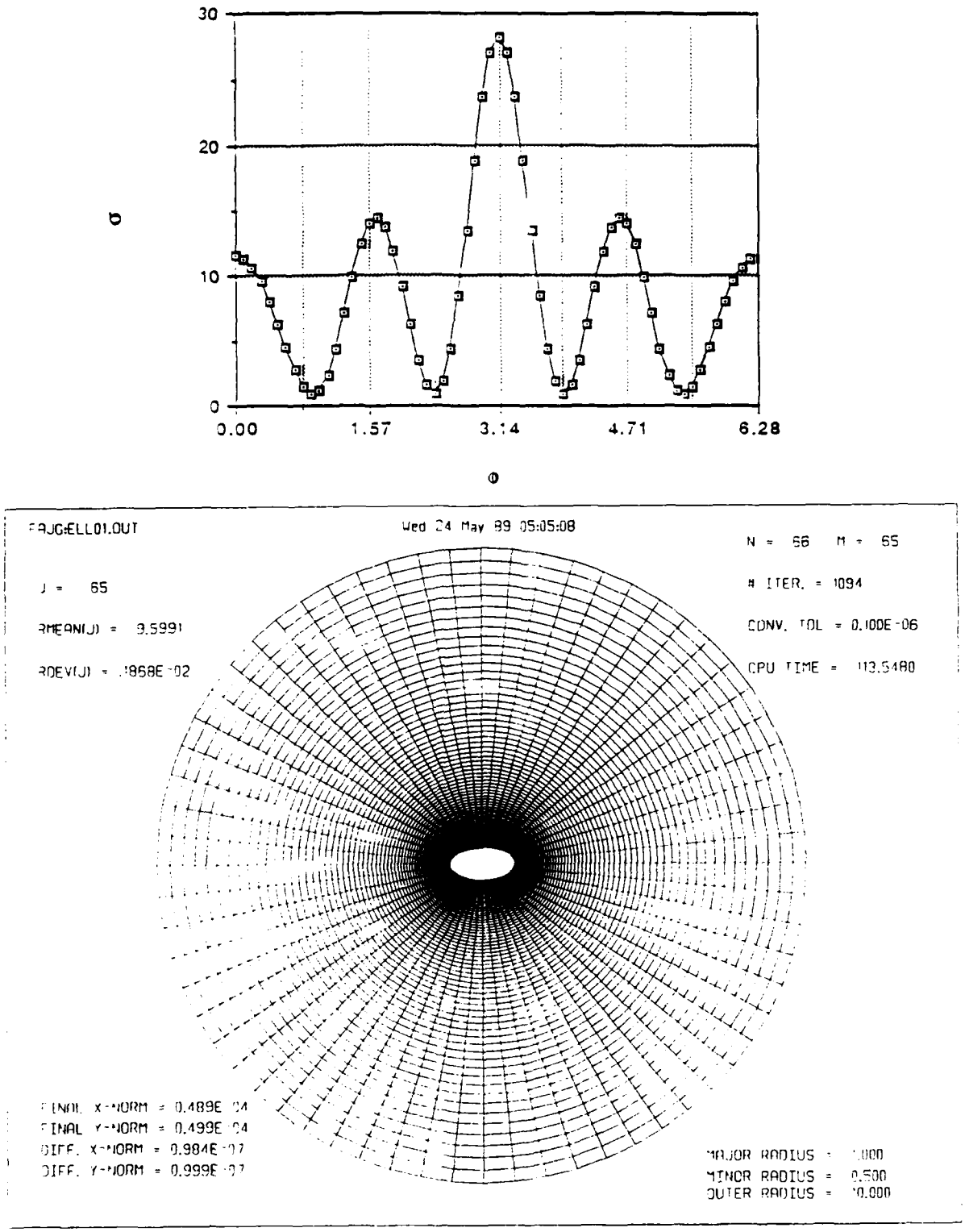

Fig. 22 Cross section of a 1x2 elliptic cylinder for ka=3 and n=6 modes.

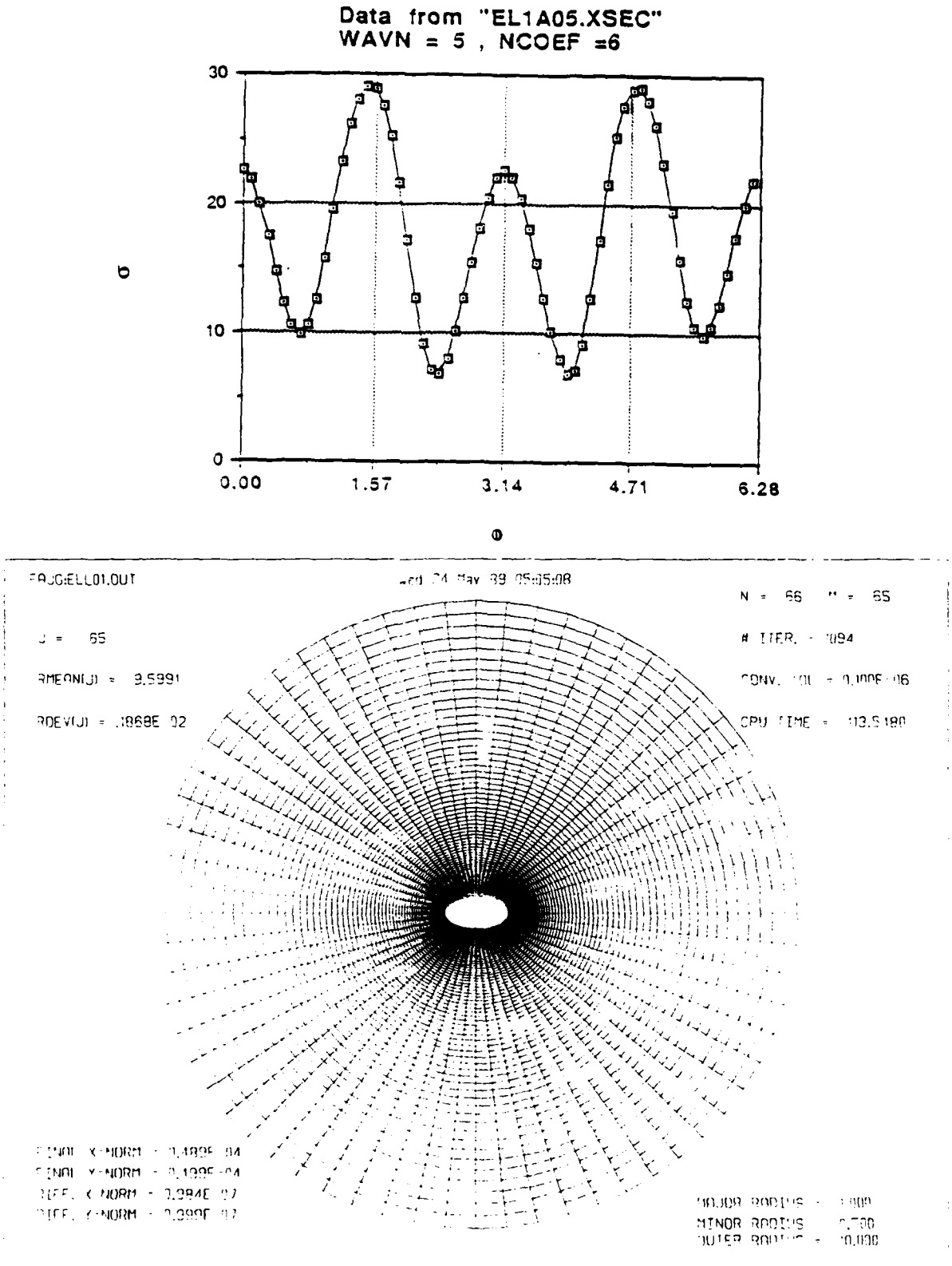

Fig. 23 Cross section of a 1x2 elliptic cylinder for ka=5 and n=6 modes.

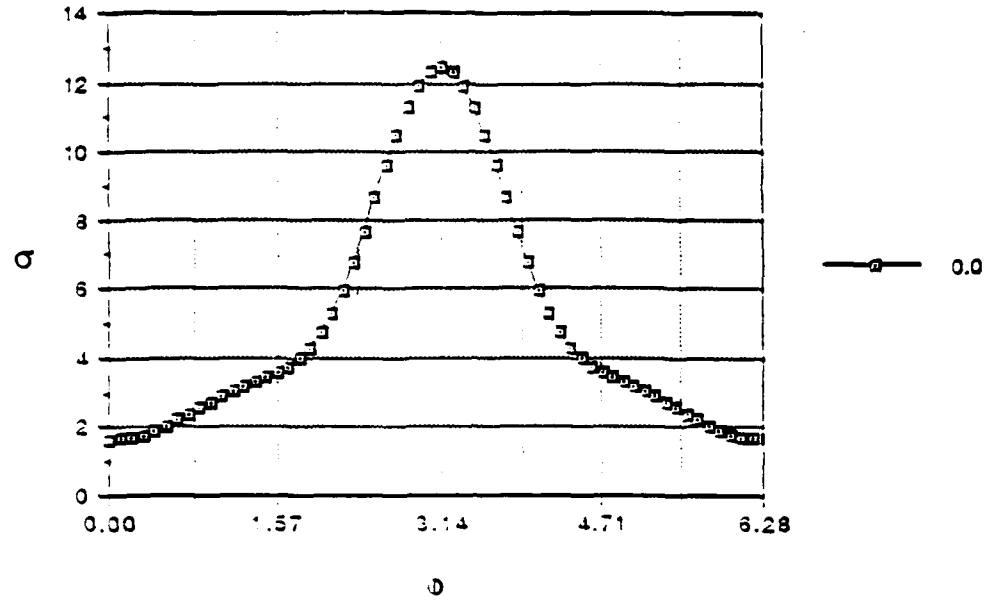

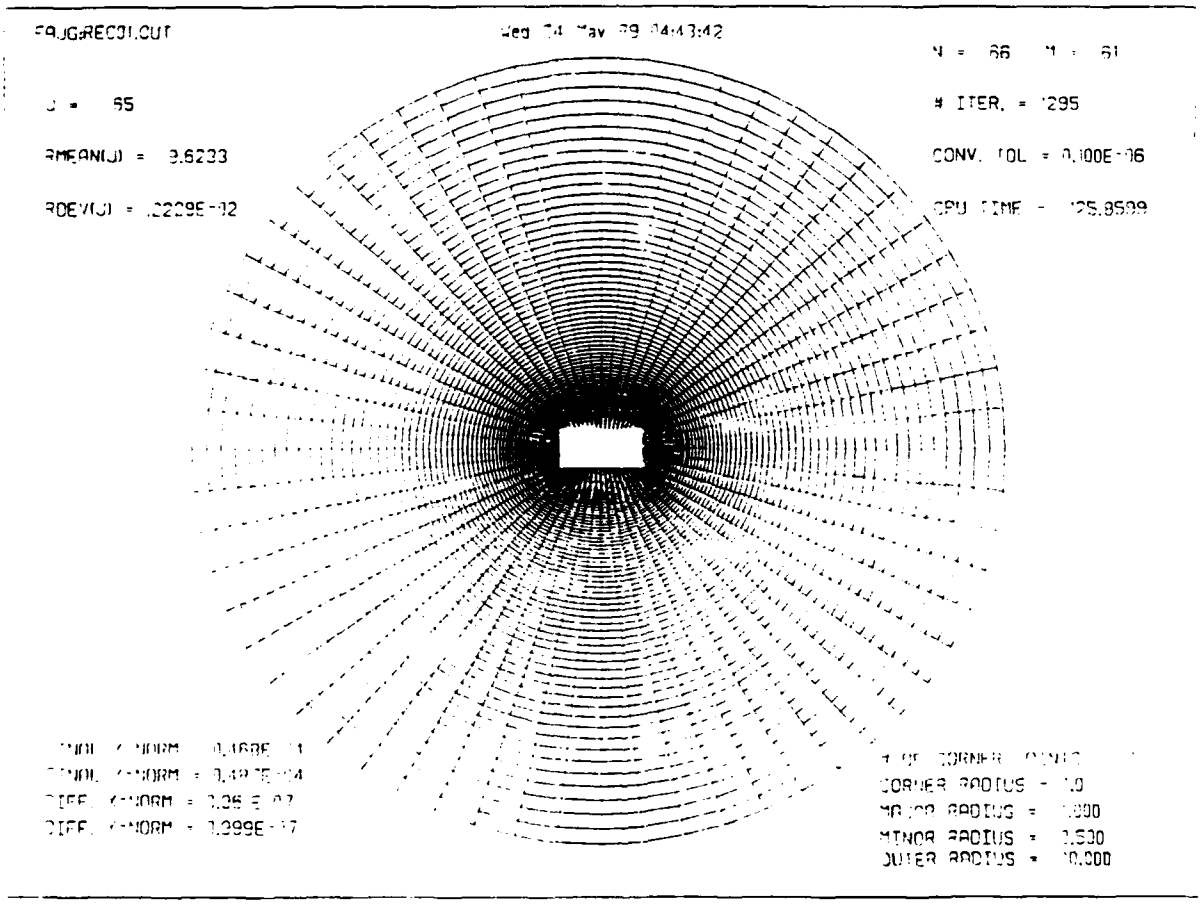

Fig. 24 Cross section of a 1x2 rectangular cylinder for ka=1 and n=4.

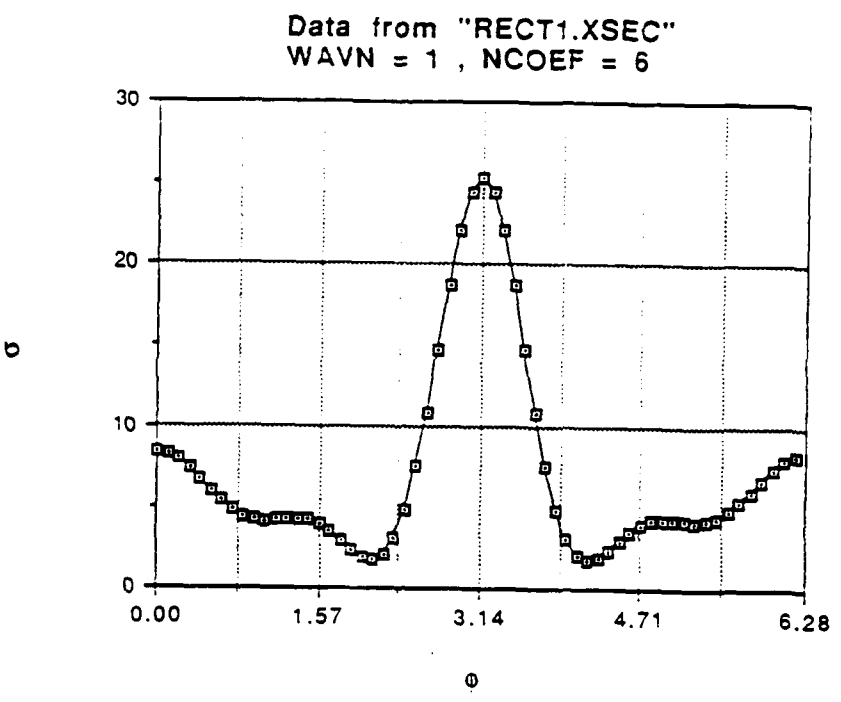

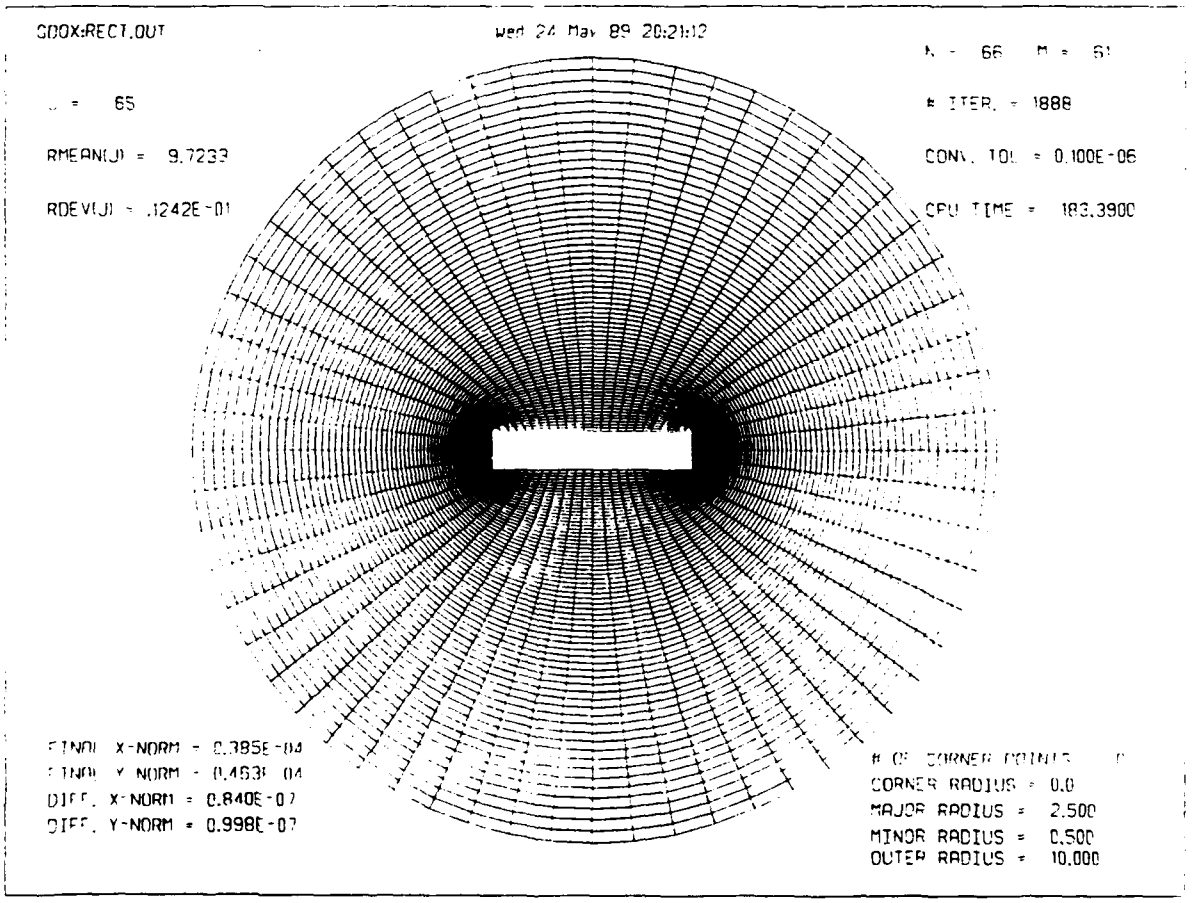

Fig. 25 Cross section of a 1x4 rectangular cylinder for ka=1 and n=4.

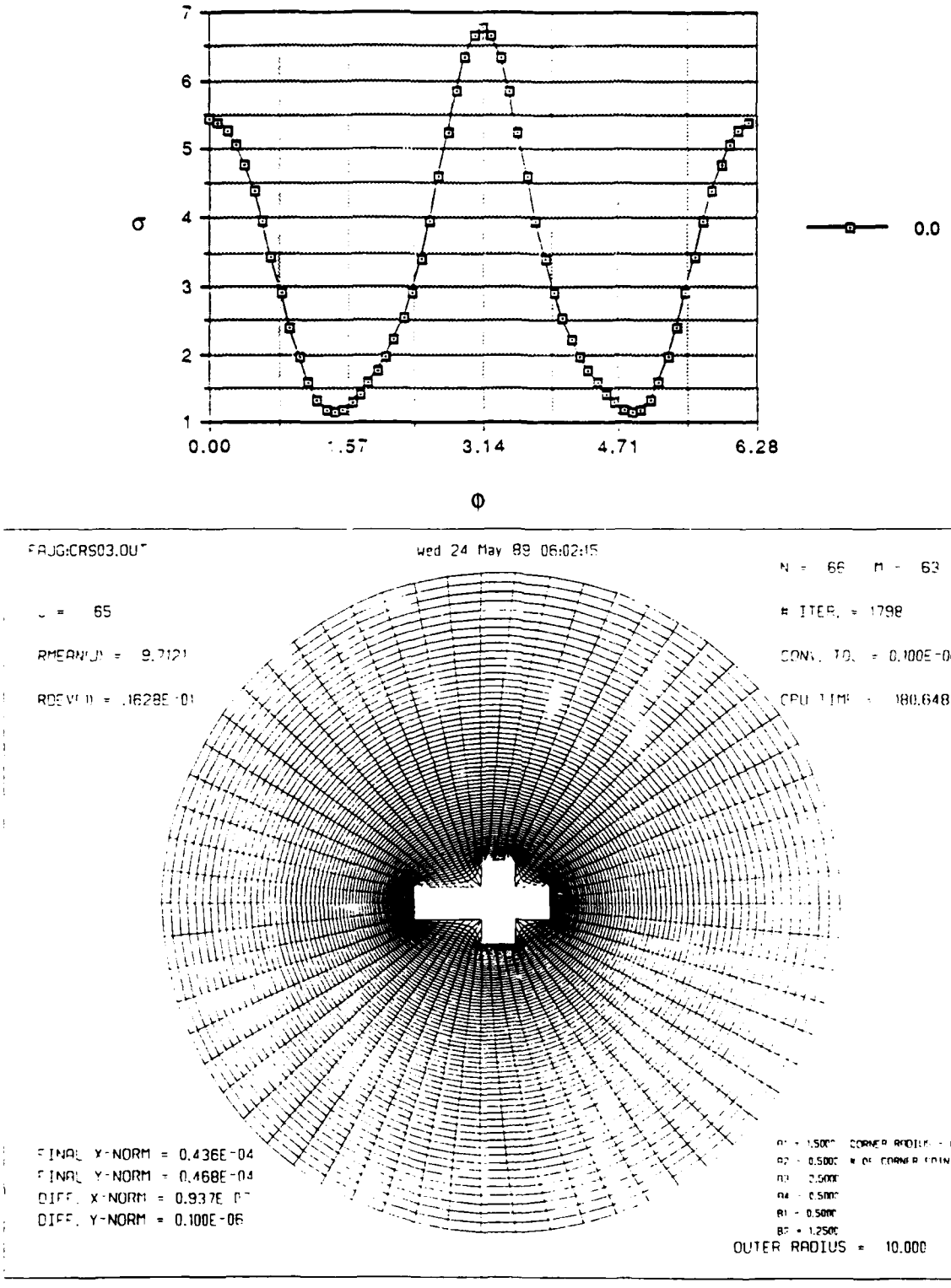

Fig. 26 Cross section of a short arm geometric cross, for ka=1 and n=4 modes.

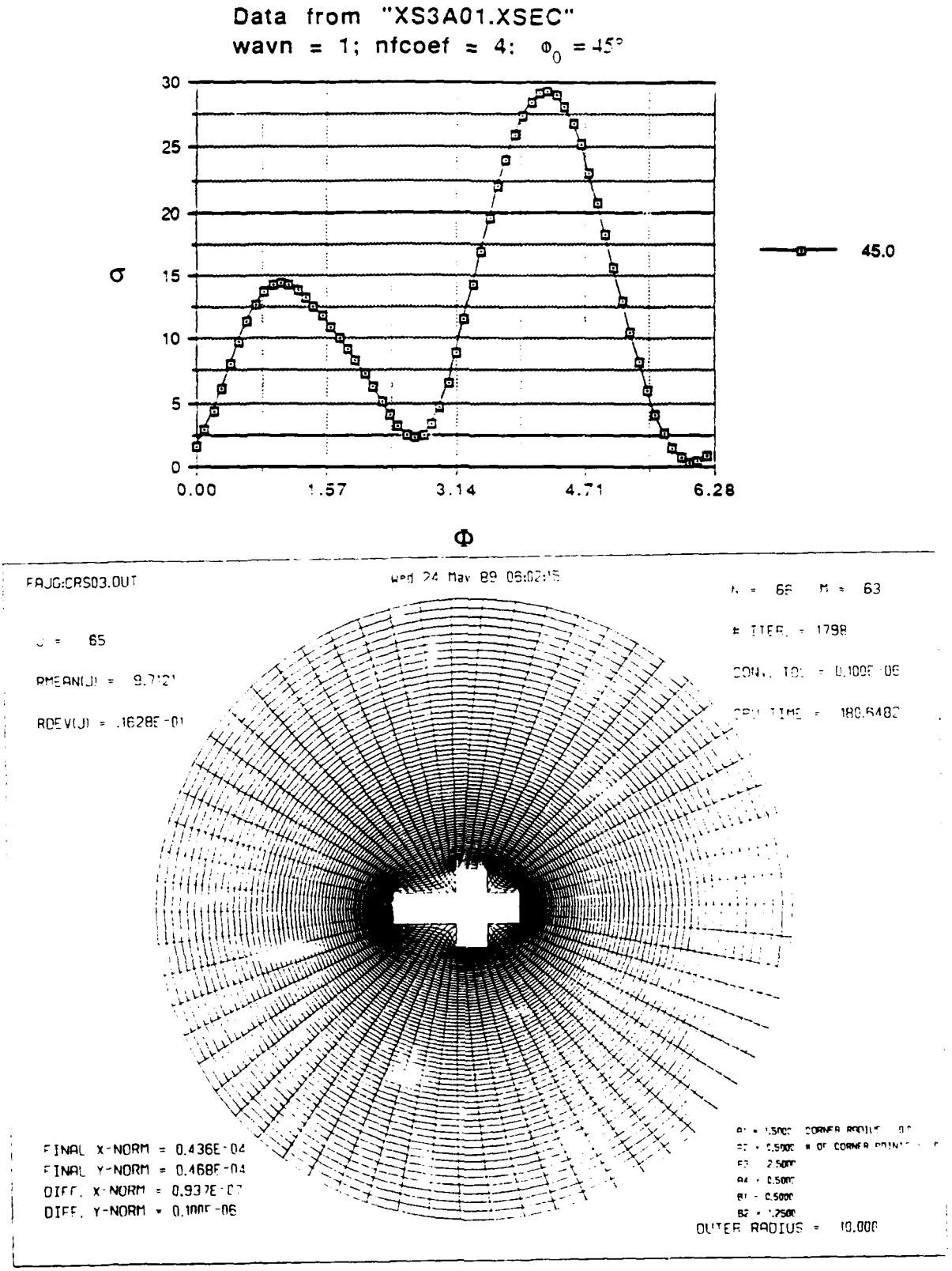

Fig. 27 Cross section of the geometric cross for ka=1 and incident angle of 45°

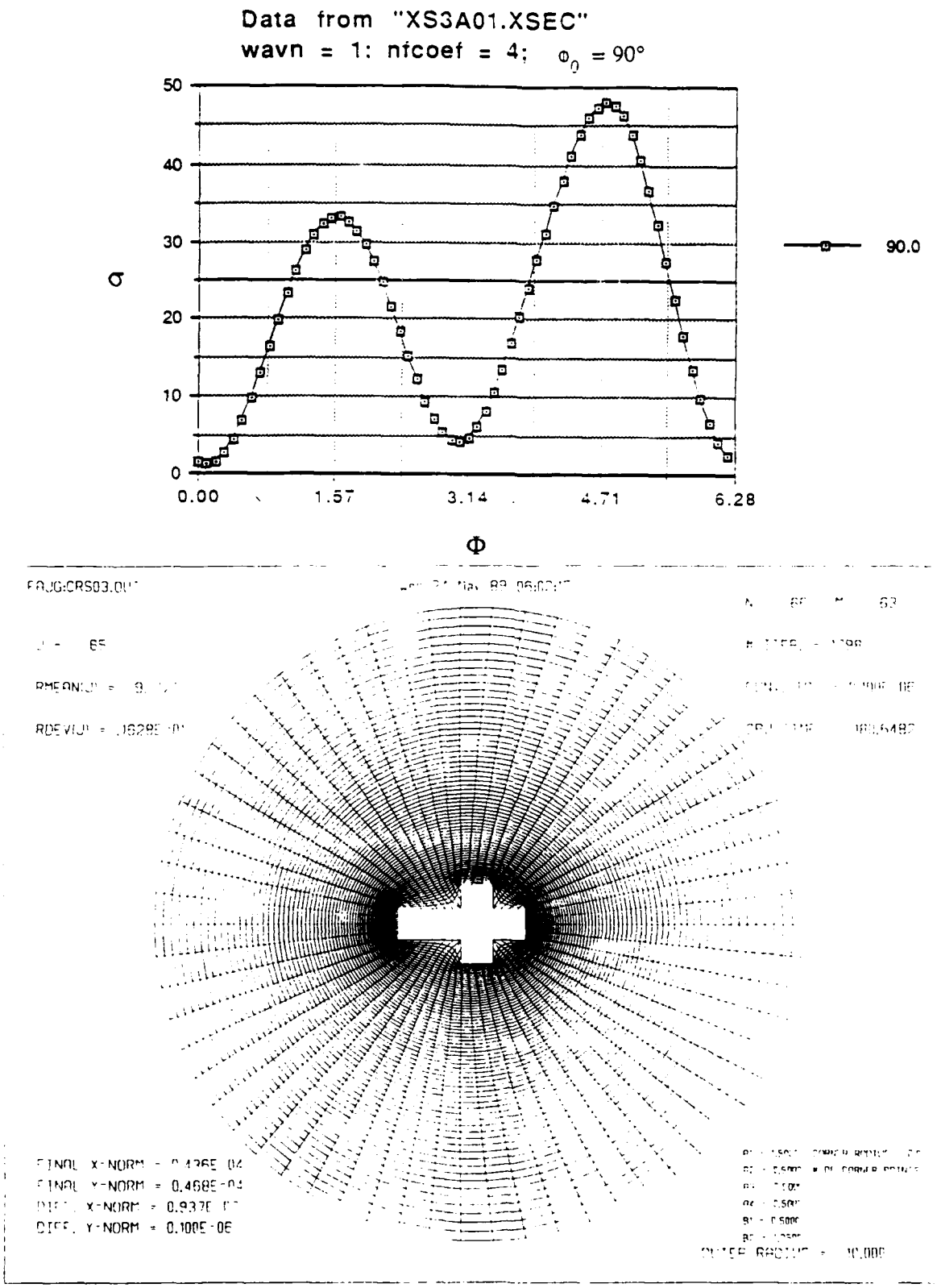

Fig. 28 Cross section of the geometric cross, for ka=1 and incident angle of 90°.

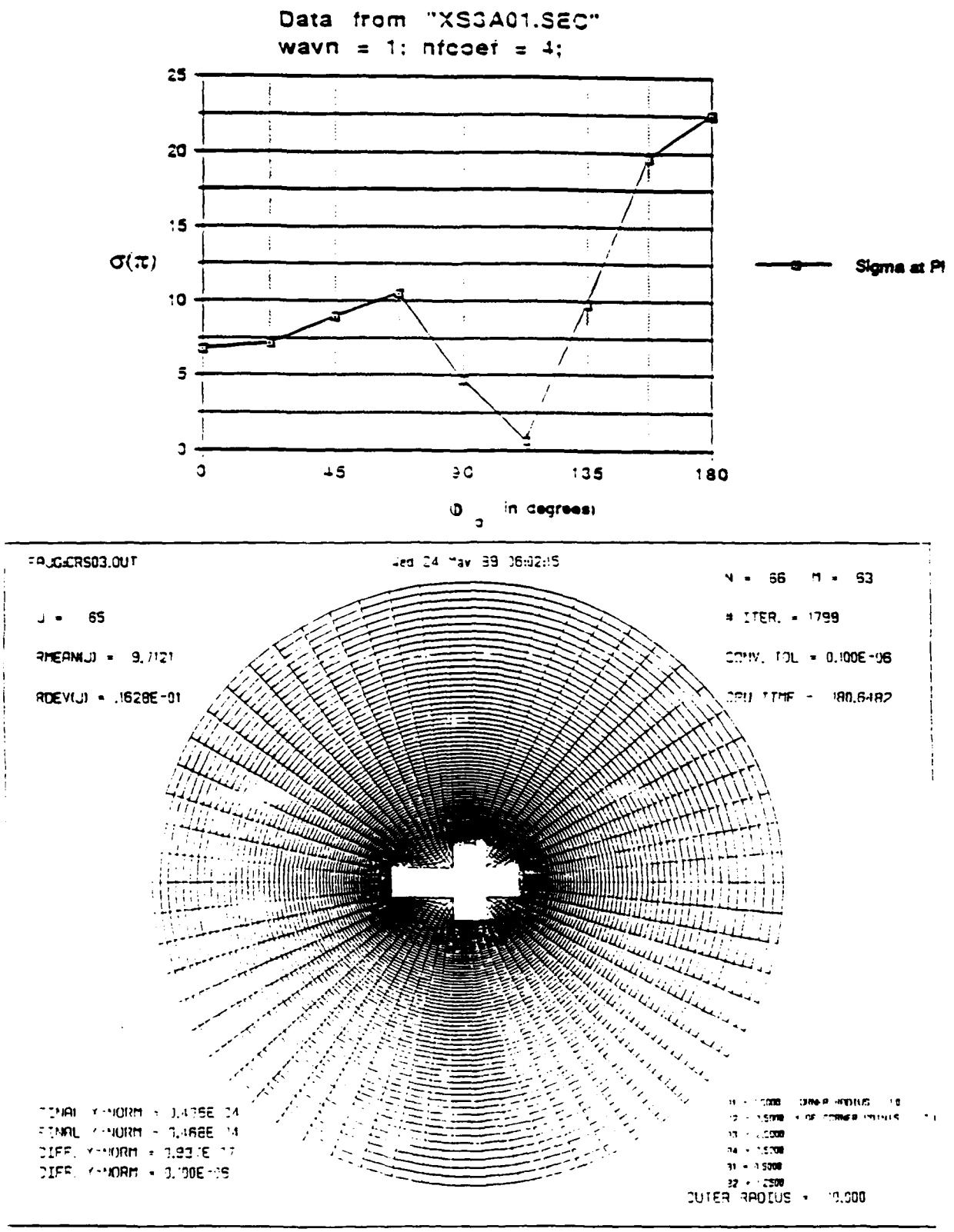

Fig. 29 Cross section at $\phi=\pi$ of the geometrical cross as a function of incident angle ϕ_0

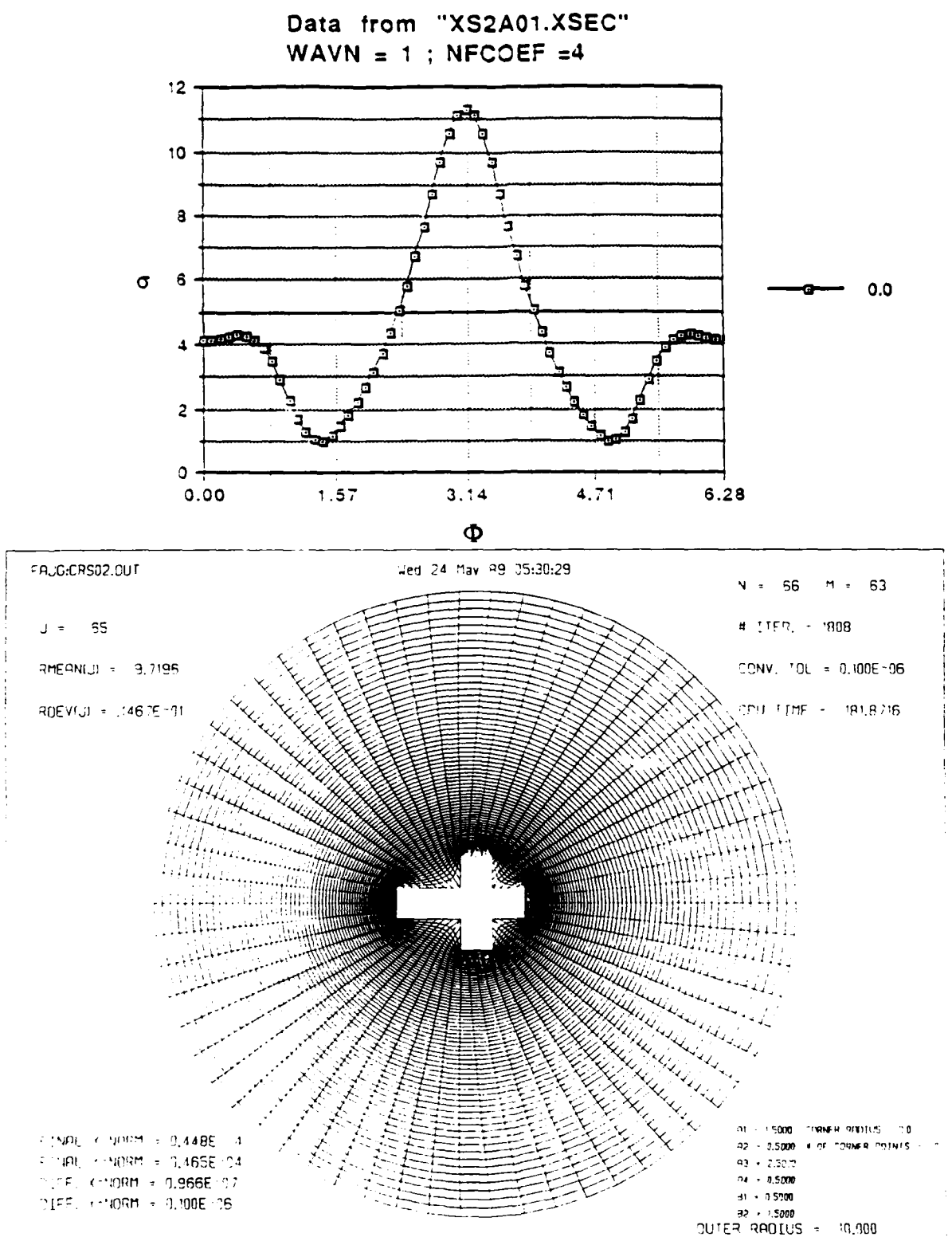

Fig. 30 Cross section of a long arm geometric cross, for ka=1 and n=4

Comparing the differential scattering cross section of an ellipse shown in Fig. 21 with that of the circle shown previously in Fig. 17 for the same wave number, we note the appearance of side lobes at right angle associated with the eccentricity of the shape. The dependence on the wave frequency for scattering by the same elliptical object under same angle of incidence can be seen by comparing Figs. 20, 21, 22 and 23.When the wavelength of the incident wave is long compared to the scale length of the scattering object, the differential scattering cross section of the ellipse resembles that of a circle for scattering of higher frequency of waves. As the wavelength becomes comparable with the scale length, the forward scattering cross section rises dramatically by an order of magnitude and side lobes appear at right angle.

The effect of the length of the scattering object along the direction of incidence can be seen by comparing Figs 24 and 25 for two rectangles of different length. The magnitude of the forward scattering cross section scales approximately linearly with the length of the object while the percent increase in the backward scattering cross section is much more pronounced. Referring back to the cross section of the ellipse shown in Fig. 21 which has similar aspect ratio as the rectangle in Fig. 24, we note that in fact, the characteristics of their differential scattering cross sections are quite different.

The relative effects of pretruding arms on the scattering cross section compared to length can be deduced by comparing Fig. 25 for the long rectangle with Fig. 26 for a short arm cross and Fig. 30 for a long arm cross. The most notable feature is that increasing the length of the body results in a significantly larger increase in the forward scattering cross section than the effect of stubby pretruding

side arms. Furthermore, increasing the length of the side arms increases the forward scattering cross section but reduces the backward scattering cross section, which is somewhat counter intuitive. The effect of the angle of incidence on the scattering cross section is evaluated by comparing Figs. 26, 27, and 28 as the angle of incidence is increased from 0 to 90 degrees at 45 degree intervals. The general trend is that magnitude of the cross section increases as the angle of incidence is increased from 0 to 90 degrees. The forward scattering cross section as a function of angle of incidence is shown plotted in Fig. 29. It should be emphasized that this figure should be interpreted with some care because when the angle of incidence in 180 degrees, the "forward" direction is actually the backward direction.

IV. CONCLUSIONS

The present work was carried out under the Small Business Innovation Research Phase I program which is limited to six months in duration at approximately one-third man-year level of effort. Under this effort, we have successfully demonstrated the concept of using a natural coordinate system that conforms to objects of arbitrary shape for the calculation of radar cross sections of such objects. The resulting algorithm is shown to be highly versatile, efficient and accurate. The present code is limited to treating two dimensional objects of arbitrary shape to establish the scientific and technical merit of the concept. The formulation, however, is completely general and can be extended directly to the full three dimensional case.

Making use of the code, we have evaluated the radar cross section for a variety of shapes. Comparison with known analytical results for an infinite cylinder showed excellent agreement. Reason for good agreement is also established. To fully test the code, the differentially radar cross section

for a variety of shapes were calculated by systematic variation of the key parameters. Upon examining the results, signatures associated with the different shapes can readily be identified, suggesting techniques for reducing radar cross sections.

The generalization of the code to three dimensions is the logical next step that can lead to the availability of a robust and efficient code for the calculation of radar cross sections.

APPENDIX

APPENDIX A

GENERATION OF NATURAL COORDINATE SYSTEM

A.1 Mathematical Formulation.

A general method of generating natural coordinate system is to let the natural coordinates be solutions of an elliptic partial differential system in the physical plane, with Dirichlet boundary conditions on all boundaries. The procedure is not restricted to two dimensions, and allows the coordinate tangential to the boundary to be distributed quite easily as desired along the boundary, and is applicable to all multiconnected regions. The coordinate system so generated is not necessarily orthogonal, but orthogonality is not required, and its lack only requires that the governing equations of the physical system must be transformed directly through implicit partial differentiation rather than by use of the scale factors and differential operators developed for orthogonal curvilinear systems. An orthogonal system cannot be achieved with arbitrary spacing of the natural coordinate lines around the boundary, and the capability for such arbitrry spacing is of more importance than orthogonality.

The objective is to transform the two dimensional, double connected region, R, bounded by two closed countours of arbitrary shape into a rectangular region, R' , as shown in Fig.1. The general transformation from the physical plane (x,y) to the transformed plane (ξ,η) is given by

$$\begin{bmatrix}\xi\\ \eta\end{bmatrix} = \begin{bmatrix}\xi(x,y)\\ \eta(x,y)\end{bmatrix} \qquad (a.1)$$

Similarly, the inverse transformation of (a.1) is

$$\begin{bmatrix} x \\ y \end{bmatrix} = \begin{bmatrix} x(\xi,\eta) \\ y(\xi,\eta) \end{bmatrix} \tag{a.2}$$

with the Jacobian matrix

$$J_2 = \begin{bmatrix} x_\xi & x_\eta \\ y_\xi & y_\eta \end{bmatrix} \tag{a.3}$$

which yields the Jacobian of the transformation

$$J = x_\xi y_\eta - x_\eta y_\xi \tag{a.4}$$

The partial derivatives of a generic function f (x,y) are transformed by

$$f_x = \frac{\partial(f,y)}{\partial(\xi,\eta)} \Big/ \frac{\partial(x,y)}{\partial(\xi,\eta)} = \frac{y_\eta f_\xi - y_\xi f_\eta}{J} \tag{a.5}$$

$$f_y = \frac{\partial(x,f)}{\partial(\xi,\eta)} \Big/ \frac{\partial(x,y)}{\partial(\xi,\eta)} = \frac{-x_\eta f_\xi - x_\xi f_\eta}{J} \tag{a.6}$$

Since the basic idea of the transformation is to generate transformation functions such that all boundaries are coincident with coordinate lines, the natural coordinates (ξ,η) are taken as solutions of some suitable elliptic boundary value problem with one of these coordinates constant on the boundaries. Using Laplace's equation as the generating elliptic system, we have

$$\xi_{xx} + \xi_{yy} = 0 \tag{a.7}$$

$$\eta_{xx} + \eta_{yy} = 0 \tag{a.8}$$

with Dirichlet boundary conditions, η = constant = η_1 on C_1, η = constant = η_2 on C_3; $\xi(x,y)$ a multiple valued solution with a branch of $\xi(x,y)$ specified (but not constant) on C_1 and C_3. The curve C_1 on the physical plane transforms to the upper boundary, C_1', of the transformed plane. Similarly, C_3 transforms to C_3', etc. The right and left boundaries of the rectangular transformed plane, C_2' and C_4', are coincident in the physical plane. The curve which transforms to these boundaries connects C_1 and C_3 and determines a branch cut for the multiple valued function $\xi(x,y)$. Thus the functions and all derivatives are continous across this cut.

Now since we wish to do all numerical computation in the rectangular transformed plane, it is necessary to interchange the dependent and independent variables in (a.7) and (a.8). Thus, using the partial derivative transformations and the chain rule, equation (b.13) in Appendix B yields

$$\alpha x_{\xi\xi} - 2\beta x_{\xi\eta} + \gamma x_{\eta\eta} = 0 \qquad \text{(a.9)}$$

$$\alpha y_{\xi\xi} - 2\beta y_{\xi\eta} + \gamma y_{\eta\eta} = 0 \qquad \text{(a.10)}$$

where the coefficients α, β and γ correspond to the components of the metric tensor of the coordinate transformation, and are given by

$$\alpha = x_\eta^2 + y_\eta^2 \qquad \text{(a.11)}$$

$$\beta = x_\xi x_\eta + y_\xi y_\eta \qquad \text{(a.12)}$$

$$\gamma = x_\xi^2 + y_\xi^2 \qquad \text{(a.13)}$$

with the transformed boundary conditions given by

$$\begin{bmatrix} x \\ y \end{bmatrix} = \begin{bmatrix} f_1(\xi,\eta_1) \\ f_2(\xi,\eta_1) \end{bmatrix} \quad , (\xi,\eta_1) \in C_1' \tag{a.14}$$

$$\begin{bmatrix} x \\ y \end{bmatrix} = \begin{bmatrix} g_1(\xi,\eta_2) \\ g_2(\xi,\eta_2) \end{bmatrix} \quad , (\xi,\eta_2) \in C_3'$$

This system is a quasi-linear elliptic system with Dirichlet boundary conditions for the physical coordinates in the transformed plane. The differential equations of the system (a.9) and (a.10) are considerably more complicated than those of Eqs.(a.7) and (a.8). However, in the first case the transformed boundary conditions are specified on straight boundaries, and the computation region is rectangular. We have thus exchanged a problem having simple equations but complex boundary conditions for a problem having complex equations and simple boundary conditions. This statement also holds for all partial differential equations which govern the physical system solved on the natural coordinates.

The natural coordinate system so generated has a constant η-line coincident with each boundary in the physical plane. The ξ-lines may be spaced in any manner desired around the boundaries by specification of the ξ boundary conditions, or equivalent by specification of (x,y) at the equi-spaced ξ-points on the η_1 and η_2 lines of the transformed plane. Control of the spacing of the η-lines may be exercised by varying the elliptic system of which ξ and η are solutions.

As noted above, orthogonality is not required of the coordinate system for solution of a system of partial differential equations. Indeed, normal derivatives on the boundaries may be easily represented in a non-orthogonal

system as follows: Let y= g(x), i.e., y-g(x)= f(x,y)=0, be the equation of some boundary in cartesian coordinates. Then

$$\frac{\partial f}{\partial n} = \mathbf{n}.\nabla f = \frac{1}{J\,(1+(g')^2)^{1/2}} \left[f_\xi (g' y_\eta + x_\eta) - f_\eta (g' y_\xi + x_\xi) \right] \qquad \text{(a.15)}$$

where g' = dy/dx. All derivatives in the last expression can be calculated along coordinate lines in the natural coordinate system. Thus it is not necessary to require orthogonality at the body surface in order to get accurate representation of the normal derivative.

A.2 Numerical Method.

The numerical solution of the system of Eqs. (a.9) and (a.10), with the boundary conditions given by Eqs. (a.14), is accomplished by the use of a nine-point finite difference approximation. The diagram in Fig.(a.1) shows the nodal arrangement for the approximation, and the paramater D is the separation between adjacent nodes. Now using central differences to aproximate the partial derivatives of the variables x and y with respect to ξ and η we obtain the following expressions:

$$x_{\xi\xi} \approx \frac{x_E - 2x_C + x_W}{\Delta^2} \qquad \text{(a.16)}$$

$$x_{\xi\eta} \approx \frac{x_{NE} - x_{NW} - x_{SE} + x_{SW}}{4\Delta^2} \qquad \text{(a.17)}$$

$$x_{\eta\eta} \approx \frac{x_N - 2x_C + x_S}{\Delta^2} \qquad \text{(a.18)}$$

$$x_\xi \approx \frac{x_E - x_W}{2\Delta} \qquad \text{(a.19)}$$

$$x_\eta \approx \frac{x_N - x_S}{2\Delta} \qquad \text{(a.20)}$$

And substituting the above expressions into Eqs.(a.9) through (a.14), we obtain

$$x_C = \frac{\alpha(x_E + x_W) - 0.5\beta(x_{NE} - x_{NW} - x_{SE} + x_{SW}) + \gamma(x_N + x_S)}{2(\alpha + \gamma)} \qquad (a.21)$$

$$y_C = \frac{\alpha(y_E + y_W) - 0.5\beta(y_{NE} - y_{NW} - y_{SE} - y_{SW}) + \gamma(y_N + y_S)}{2(\alpha + \gamma)} \qquad (a.22)$$

where

$$\alpha = (x_N - x_S)^2 + (y_N - y_S)^2 \qquad (a.23)$$

$$\beta = (x_E - x_W)(x_N - x_S) + (y_E - y_W)(y_N - y_S) \qquad (a.24)$$

$$\gamma = (x_E - x_W)^2 + (y_E - y_W)^2 \qquad (a.25)$$

The above system will now be solved on the (ξ,η) rectangular plane with $\xi_i = i$, for i = 1, 2, ... ,M-1 and $\eta_j = j$, for j = 1, 2, ... ,N. There are 4(M-1) known values corresponding to the x and y points at the boundaries, and therefore there are 2(N-2)(M-1) unknown values to be determined. We will use Gauss-Seidel iteration scheme, which is a direct substitution method using updated values as they are generated in an iteration.

The values of x and y on the left and right boundaries of the transformed plane, C_2' and C_4', are unknown but continuous in η. This implies that the values of x_W, x_{SE} and x_{NE} at i=M-1 are also the values i =1. These relations also hold for the y-values at those boundaries. A good initial guess is needed to obtain convergence in Gauss-Seidel method. Since the x's and y's in the radial direction will fall between the values at the boundaries it seems that a weighted average of these values constitutes an appropriate guess. Therefore, the values for x_{ij} and y_{ij} can be evaluated from

$$x_{ij} = \frac{1}{2}\left\{\left(\frac{N-j}{N-1}\right)x_{i1} + \left(\frac{j-1}{N-1}\right)x_{iN}\right\} \qquad \text{(a.26)}$$

$$y_{ij} = \frac{1}{2}\left\{\left(\frac{N-j}{N-1}\right)y_{i1} + \left(\frac{j-1}{N-1}\right)y_{iN}\right\} \qquad \text{(a.27)}$$

where j= 2,3,...,N-1 and i=1,2,...,M-1.

Comparison of the difference of the absolute norm of the k^{th} and k - 1^{st} iterations was used for checking convergence. The || x || is calculated by

$$\|x\|^{(k)} = \frac{\sum_{j=2}^{N-1}\sum_{i=1}^{M-1} | x_{ij}^{(k)} - x_{ij}^{(k-1)} |}{(M-1)(N-2)} \qquad \text{(a.28)}$$

where the difference in the norms is calculated as

$$\text{Diff. } \|x\| = | \|x\|^{(k)} - \|x\|^{(k-1)} | \qquad \text{(a.29)}$$

And similarly for the difference in the y-norm. If the difference in the norms is less than a given tolerance the iteration process converges and the final values for x and y will define the grid points corresponding to the (ξ,η) coordinates.

The set of finite difference Eqs.(a.21) and (a.22) has been successfully solved for a number of two dimensional objects with various geometric cross sections corresponding to circles, ellipses, rectangles and even more arbitrary geometries. For all these cases the outer boundary is defined by a perfect circle, as desired by the matching interface in

the scattering problem. The plots shown are of ξ = constant lines and η = constant lines in the physical plane.

The specification of the convergence tolerance was found to be dependent on the number of iterations. The number of iterations as a function of convergence tolerance has the form of $ce^{-1/x}$ (where x = convergence tolerance). A false convergence was found when the number of iterations was below 150. This implies that the convergence tolerance must be at most $O(10^{-4})$. Also the N-1 contour is required to be cylindrical which implies that the deviation in the radius must be small. A convergence tolerance of $O(10^{-7})$ satisfied both of the above criterion.

It was observed that the number of points per contour had a more significant effect on the cost of generation than did the number of contours. The doubling of the number of contours increased the number of iterations by less than 5%. The doubling of the number of points per contour doubled the number of iterations required. It was also observed that the greater the number of contours the better the resolution near the inner boundary.

APPENDIX B

Transformation Algorithm

I. Derivatives and Vectors in the Transformed Plane

Given that $x=x(\xi,\eta)$ and $y=y(\xi,\eta)$ we obtain a set of relations in the transformed (x,h) plane. Let $f = f(x,y)$ - a twice differentiable scalar function of x and y.

$$|J| = x_\xi y_\eta - x_\eta y_\xi$$

By the chain rule we obtain

$$\begin{pmatrix} f_\xi \\ f_\eta \end{pmatrix} = \begin{pmatrix} x_\xi & y_\xi \\ x_\eta & y_\eta \end{pmatrix} \begin{pmatrix} f_x \\ f_y \end{pmatrix} = J^t \begin{pmatrix} f_x \\ f_y \end{pmatrix}$$

Thus,

$$\begin{pmatrix} f_x \\ f_y \end{pmatrix} = \frac{1}{|J|} \begin{pmatrix} y_\eta & -y_\xi \\ -x_\eta & x_\xi \end{pmatrix} \begin{pmatrix} f_\xi \\ f_\eta \end{pmatrix} \qquad \text{(b.1)}$$

where $|J| = \det J$.

With another application of the chain rule we obtain

$$\begin{pmatrix} f_{\xi\xi} \\ f_{\xi\eta} \\ f_{\eta\eta} \\ f_\xi \\ f_\eta \end{pmatrix} = M \begin{pmatrix} f_{xx} \\ f_{xy} \\ f_{yy} \\ f_x \\ f_y \end{pmatrix}$$

where

$$M = \begin{pmatrix} & A & & B \\ 0 & 0 & 0 & \\ 0 & 0 & 0 & J^t \end{pmatrix}$$

$$A = \begin{pmatrix} x_\xi^2 & 2x_\xi y_\xi & y_\xi^2 \\ x_\xi x_\eta & x_\xi y_\eta + x_\eta y_\xi & y_\xi y_\eta \\ x_\eta^2 & 2x_\eta y_\eta & y_\eta^2 \end{pmatrix}$$

$$B = \begin{pmatrix} x_{\xi\xi} & y_{\xi\xi} \\ x_{\xi\eta} & y_{\xi\eta} \\ x_{\eta\eta} & y_{\eta\eta} \end{pmatrix}$$

$$\det M = \det A \cdot |J| = |J|^4$$

By inverting the 5x5 matrix M we obtain the relations between the derivatives of f in the x-y plane with respect to the derivatives in the x-h plane.

$$\begin{pmatrix} f_{xx} \\ f_{xy} \\ f_{yy} \\ f_x \\ f_y \end{pmatrix} = M^{-1} \begin{pmatrix} f_{\xi\xi} \\ f_{\xi\eta} \\ f_{\eta\eta} \\ f_\xi \\ f_\eta \end{pmatrix} \qquad \text{(b.2)}$$

where

$$M^{-1} = \frac{1}{|J|^3} \begin{pmatrix} & |J| \cdot C & & D \\ 0 & 0 & 0 & \\ 0 & 0 & 0 & |J|^3 (J^t)^{-1} \end{pmatrix}$$

$$C = \begin{pmatrix} y_\eta^2 & 2y_\xi y_\eta & y_\xi^2 \\ -x_\eta y_\eta & x_\xi y_\eta + x_\eta y_\xi & -x_\xi y_\xi \\ x_\eta^2 & -2x_\xi x_\eta & x_\xi^2 \end{pmatrix}$$

$$D = \begin{pmatrix} x_\eta a - y_\eta b & -x_\xi a + y_\xi b \\ -x_\eta c + y_\eta d & x_\xi c - y_\xi d \\ x_\eta e - y_\eta g & -x_\xi e + y_\xi g \end{pmatrix}$$

where

$$a = y_\xi^2 y_{\eta\eta} - 2y_\xi y_\eta y_{\xi\eta} + y_\eta^2 y_{\xi\xi}$$

$$b = y_\xi^2 x_{\eta\eta} - 2y_\xi y_\eta x_{\xi\eta} + y_\eta^2 x_{\xi\xi}$$

$$c = x_\eta y_\eta y_{\xi\xi} - (x_\xi y_\eta + x_\eta y_\xi) y_{\xi\eta} + x_\xi y_\xi y_{\eta\eta}$$

$$d = x_\eta y_\eta x_{\xi\xi} - (x_\xi y_\eta + x_\eta y_\xi) x_{\xi\eta} + x_\xi y_\xi x_{\eta\eta}$$

$$e = x_\eta^2 y_{\xi\xi} - 2x_\xi x_\eta y_{\xi\eta} + x_\xi^2 y_{\eta\eta}$$

$$g = x_\eta^2 x_{\xi\xi} - 2x_\xi x_\eta x_{\xi\eta} + x_\xi^2 x_{\eta\eta}$$

From (1) and (2) we obtain the derivative transformations

$$f_x = \left(\frac{\partial f}{\partial x}\right) = \frac{(y_\eta f_\xi - y_\xi f_\eta)}{|J|} \qquad \text{(b.3)}$$

$$f_y = \left(\frac{\partial f}{\partial y}\right) = \frac{(x_\xi f_\eta - x_\eta f_\xi)}{|J|} \qquad \text{(b.4)}$$

$$f_{xx} = \left(\frac{\partial^2 f}{\partial x^2}\right) = \frac{(y_\eta^2 f_{\xi\xi} - 2y_\xi y_\eta f_{\xi\eta} + y_\xi^2 f_{\eta\eta})}{|J|^2} + \qquad \text{(b.5)}$$

$$\frac{[a(x_\eta f_\xi - x_\xi f_\eta) + b(y_\xi f_\eta - y_\eta f_\xi)]}{|J|^3}$$

$$f_{yy} = \left(\frac{\partial^2 f}{\partial y^2}\right) = \frac{(x_\eta^2 f_{\xi\xi} - 2x_\xi x_\eta f_{\xi\eta} + x_\xi^2 f_{\eta\eta})}{|J|^2} + \qquad \text{(b.6)}$$

$$\frac{[e(x_\eta f_\xi - x_\xi f_\eta) + g(y_\xi f_\eta - y_\eta f_\xi)]}{|J|^3}$$

$$f_{xy} = \frac{[(x_\xi y_\eta + x_\eta y_\xi) f_{\xi\eta} - x_\xi y_\xi f_{\eta\eta} - x_\eta y_\eta f_{\xi\xi}]}{|J|^2} + \qquad \text{(b.7)}$$

$$\frac{[d(y_\eta f_\xi - y_\xi f_\eta) + c(x_\xi f_\eta - x_\eta f_\xi)]}{|J|^3}$$

The Laplacian is

$$\nabla^2 f = \frac{(\alpha f_{\xi\xi} - 2\beta f_{\xi\eta} + \gamma f_{\eta\eta})}{|J|^2} + \qquad \text{(b.8)}$$

$$\frac{[(\alpha x_{\xi\xi} - 2\beta x_{\xi\eta} + \gamma x_{\eta\eta})(y_\xi f_\eta - y_\eta f_\xi)]}{|J|^3} +$$

$$\frac{(\alpha y_{\xi\xi} - 2\beta y_{\xi\eta} + \gamma y_{\eta\eta})(x_\eta f_\xi - x_\xi f_\eta)}{|J|^3}$$

or

$$\nabla^2 f = \frac{\alpha f_{\xi\xi} - 2\beta f_{\xi\eta} + \gamma f_{\eta\eta} + \sigma f_\eta + \tau f_\xi}{|J|^2} \qquad \text{(b.9)}$$

where

$$\alpha = x_\eta^2 + y_\eta^2$$

$$\beta = x_\xi x_\eta + y_\xi y_\eta$$

$$\gamma = x_\xi^2 + y_\xi^2$$

$$Dx = \alpha x_{\xi\xi} - 2\beta x_{\xi\eta} + \gamma x_{\eta\eta} \qquad \text{(b.10)}$$

$$Dy = \alpha y_{\xi\xi} - 2\beta y_{\xi\eta} + \gamma y_{\eta\eta}$$

$$\sigma = \frac{y_\xi Dx - x_\xi Dy}{|J|}$$

$$\tau = \frac{x_\eta Dy - y_\eta Dx}{|J|}$$

In particular the derivatives of $\xi(x,y)$ and $\eta(x,y)$ are

$$\xi_{xx} = \frac{a x_\eta - b y_\eta}{|J|^3} \qquad \text{(b.11)}$$

$$\xi_{yy} = \frac{ex_\eta - gy_\eta}{|J|^3}$$

$$\nabla^2\xi = \frac{(a+e)x_\eta - (b+g)y_\eta}{|J|^3} = \frac{\tau}{|J|^2}$$

Similarly

$$\nabla^2\eta = \frac{\sigma}{|J|^2} \qquad \text{(b.12)}$$

If $\nabla^2\xi = 0$ and $\nabla^2\eta = 0$ then $\sigma = 0$ and $\tau = 0$ and (9) is transformed into

$$\nabla^2 f = \frac{\alpha f_{\xi\xi} - 2\beta f_{\xi\eta} + \gamma f_{\eta\eta}}{|J|^2} \qquad \text{(b.13)}$$

II. Unit Tangent and Unit Normal Vectors in the (x,h) plane

Utilizing (3) and (4) we have

$$\underline{n}^{(\eta)} = \frac{\underline{\nabla}\eta}{|\underline{\nabla}\eta|} = \frac{-y_\xi \underline{i} + x_\xi \underline{j}}{\sqrt{\gamma}} \qquad \text{(b.14)}$$

which is the unit vector normal to a line of constant h. Similarly the unit vector normal to a line of constant x is given by

$$\underline{n}^{(\xi)} = \frac{\underline{\nabla}\xi}{|\underline{\nabla}\xi|} = \frac{y_\eta \underline{i} - x_\eta \underline{j}}{\sqrt{\alpha}} \qquad \text{(b.15)}$$

The unit tangent vectors are given by

$$\underline{t}^{(\eta)} = \underline{n}^{(\eta)} \times \underline{k} = \frac{x_\xi \underline{i} + y_\xi \underline{j}}{\sqrt{\gamma}} \qquad \text{(b.16)}$$

$$\underline{t}^{(\xi)} = \underline{n}^{(\xi)} \times \underline{k} = \frac{-(x_\eta \underline{i} + y_\eta \underline{j})}{\sqrt{\alpha}}$$

APPENDIX C

METHOD OF SOLUTION FOR FINDING FOURIER COEFFICIENTS

Because of the linearity of the governing equations, we can write the total field, E_{tot}, as the sum of an incident field and a scattered field.

$$E_{tot} = E_{in} + E_s$$

$$E_{in} = e^{-ikr\cos(\phi-\phi_0)}$$

$$E_s = \sum_{m=-\infty}^{+\infty} A_m H_m(kr) e^{im\phi}$$

The constants, A_m, are generally complex. H_m are cylindrical Hankel Functions of the first kind of order m:

$$H_m = J_m + iY_m$$

and $$e^{im\phi} = \cos(m\phi) + i\sin(m\phi)$$

On the inside boundary

$$E_{tot} = 0, \text{ therefore, } E_s = -E_{in}$$

The scattered field can be broken down into a real and imaginary part:

$$(E_s)_R = \sum_{m=-\infty}^{+\infty} [a_m J_m - b_m Y_m]\cos(m\phi) - [a_m Y_m + b_m J_m]\sin(m\phi)$$

$$(E_s)_I = \sum_{m=-\infty}^{+\infty} [a_m Y_m + b_m J_m]\cos(m\phi) + [a_m J_m - b_m Y_m]\sin(m\phi)$$

It is desirable to combine terms so that the summation is over positive integers.

$$(E_s)_R = [a_o J_o - b_o Y_o]$$
$$+ \sum_{m=1}^{+\infty} [a_m J_m + a_{-m}(-1)^m J_m - b_m Y_m - b_{-m}(-1)^m Y_m] \cos(m\phi)$$
$$- \sum_{m=1}^{+\infty} [a_m Y_m - a_{-m}(-1)^m Y_m + b_m J_m - b_{-m}(-1)^m J_m] \sin(m\phi)$$

$$(E_s)_I = [a_o Y_o + b_o J_o]$$
$$+ \sum_{m=1}^{+\infty} [a_m Y_m + a_{-m}(-1)^m Y_m + b_m J_m + b_{-m}(-1)^m J_m] \cos(m\phi)$$
$$+ \sum_{m=1}^{+\infty} [a_m J_m - a_{-m}(-1)^m J_m - b_m Y_m + b_{-m}(-1)^m Y_m] \sin(m\phi)$$

For the ideal case of an obstacle having a circular shape, these equations can be matched - equated to Fourier expansions of the boundary conditions.

For example, at r=1,

$$(E_s)_R = -\cos[k\cos(\phi - \phi_o)] \equiv f(\phi)$$

$$(E_s)_I = +\sin[k\cos(\phi - \phi_o)] \equiv g(\phi)$$

Both $f(\phi)$ and $g(\phi)$ can be expanded as Fourier series:

$$f(\phi) = A_o + \sum_{m=1}^{+\infty} A_m \cos(m\phi) + B_m \sin(m\phi)$$

$$g(\phi) = C_o + \sum_{m=1}^{+\infty} C_m \cos(m\phi) + D_m \sin(m\phi)$$

Matching mode by mode gives:

m=0

$$\begin{bmatrix} A_o \\ C_o \end{bmatrix} = \begin{bmatrix} J_o & -Y_o \\ Y_o & J_o \end{bmatrix} \begin{bmatrix} a_o \\ b_o \end{bmatrix}$$

and for m=1 to $+\infty$

$$\begin{bmatrix} A_m \\ B_m \\ C_m \\ D_m \end{bmatrix} = \begin{bmatrix} +J_m & +(-1)^m J_m & -Y_m & -(-1)^m Y_m \\ -Y_m & +(-1)^m Y_m & -J_m & +(-1)^m J_m \\ +Y_m & +(-1)^m Y_m & +J_m & +(-1)^m J_m \\ +J_m & -(-1)^m J_m & -Y_m & +(-1)^m Y_m \end{bmatrix} \begin{bmatrix} a_m \\ a_{-m} \\ b_m \\ b_{-m} \end{bmatrix}$$

If we were solving the problem in cylindrical coordinates, the unknown constants [am, a_{-m}, bm, b_{-m}] could be easily determined by solving the simple 4x4 system of linear equations.

For the general boundary shape such that

$$r_{obs} = r_i(\phi)$$

The problem is more complicated.

on r_{in},

$$(E_s)_R = -\cos[k\, r_i(\phi) \cos(\phi - \phi_o)]$$

$$(E_s)_I = +\sin[k\, r_i(\phi) \cos(\phi - \phi_o)]$$

However, in the natural coordinate system, (ξ,η), the boundary $r_i(\phi)$ corresponds to $\eta=1$. We are at liberty to define the following expansion:

$$f(\xi^*) = \tilde{A}_o + \sum_{m=1}^{+\infty} \tilde{A}_m \cos(m\xi^*) + \tilde{B}_m \sin(m\xi^*)$$

$$g(\xi^*) = \tilde{C}_o + \sum_{m=1}^{+\infty} \tilde{C}_m \cos(m\xi^*) + \tilde{D}_m \sin(m\xi^*)$$

where $$\xi^* = \left(\frac{2\pi\,(\xi-1)}{\xi_{max}}\right)$$

The constants $\tilde{A}_m$, $\tilde{B}_m$, $\tilde{C}_m$, $\tilde{D}_m$ are line/contour integrals over the boundary shape.

e.g. $$\tilde{A}_m = \frac{-1}{\pi} \int_0^{2\pi} \cos(kr(\xi^*) \cos(\phi(\xi^*) - \phi_o))\, d\xi^*$$

since $r(\xi^*)$ and $\phi(\xi^*)$ are points on the surface in the parameter ξ^*.

For this to work, we need to find functions as the following form:

$$[E_s(\xi,\eta)]_R = \sum_{m=-\infty}^{+\infty} \left\{ a_m \left[A_m^1(\xi,\eta) \cos(m\xi^*) - A_m^2(\xi,\eta) \sin(m\xi^*)\right] - b_m \left[B_m^1(\xi,\eta) \cos(m\xi^*) - B_m^2(\xi,\eta) \sin(m\xi^*)\right] \right\}$$

$$[E_s(\xi,\eta)]_I = \sum_{m=-\infty}^{+\infty} \{a_m [A^2_m(\xi,\eta)\cos(m\xi^*) + A^1_m(\xi,\eta)\sin(m\xi^*)] + b_m [B^2_m(\xi,\eta)\cos(m\xi^*) - B^1_m(\xi,\eta)\sin(m\xi^*)]\}$$

In which the general functions $A^1_m(\xi,\eta)$, $A^2_m(\xi,\eta)$, $B^1_m(\xi,\eta)$, $B^2_m(\xi,\eta)$ replace the Bessel functions used in cylindrical coordinates. We can pick the natural coordinate system in such a way that, at the outside boundary, $r=r_o$ or $\eta=\eta_{max}$, $\xi^*=\phi$.

Now if at $r=r_o$,

$$A^1_m \to J_m \qquad A^2_m \to Y_m$$

$$B^1_m \to Y_m \qquad B^2_m \to J_m$$

$$\frac{\partial(A^1_m)}{\partial r} \to \frac{dJ_m}{dr} \qquad \text{and so on}$$

and if we force:

$$H\,(A^1_m(\xi^*,\eta)\cos(m\xi^*)) = 0 \qquad H(A^2_m(\xi^*,\eta)\sin(m\xi^*)) = 0$$

then $Es(\xi,\eta)$ matches into the cylindrical coordinate system smoothly. The operator H is the Helmholtz equation in (ξ,η) space.

$$H(\psi) = \alpha\frac{\partial^2\psi}{\partial\xi^2} - 2\beta\frac{\partial^2\psi}{\partial\xi\partial\eta} + \gamma\frac{\partial^2\psi}{\partial\eta^2} + J^2k^2\psi = 0$$

The functions A^1_m, ... are generalized eigenfunctions, which are determined numerically by solving the H equation subject to proper boundary conditions. At $\eta=1$ A^1_m, ... are simply constants.

at $\eta=\eta_{max}$ $\quad A_m^1 = J_m(kr_o)$

$$\frac{\partial A_m^1}{\partial r} = \left(\frac{\partial J_m(kr)}{\partial r}\right)_{r=r_o}$$

The solution for A^1_m consists of a two point Boundary value problem which requires a shooting method under general conditions.

As an illustration, consider:

$$H(A_m^1 \cos(m\xi^*)) = 0$$

The solution procedure involves:

1. Set $(A_m^1 \cos(m\xi^*))_{\eta=\eta_{max}} = J_m(kr_o)\cos(m\xi^*)$

2. Pick an initial value for $(A_m^1)_{\eta=1} = \text{constant} = A_m^{1^*}$

3. Solve $H[A_m^1 \cos(m\xi^*)] = 0$

4. Check the slope at $r=r_o$ to see whether or not:

$$\frac{\partial(A_m^1)}{\partial r} = \frac{\partial J_m^1}{\partial r}$$

If agreement is unsatisfactory, pick a new value of A^*_m and go back to step 2.

In turn, all four functions can be generated and four general constants, $(A^1_m)^*$, $(A^2_m)^*$, which depend only on the problem geometry, are found. Now, we can match the B.C. on the obstacle at $\eta=1$ by using the following:

$$\begin{bmatrix} \tilde{A}_m \\ \tilde{B}_m \\ \tilde{C}_m \\ \tilde{D}_m \end{bmatrix} = \begin{bmatrix} +A_m^1 & +(-1)^m A_m^1 & -B_m^1 & -(-1)^m B_m^1 \\ -A_m^2 & +(-1)^m A_m^2 & -B_m^2 & +(-1)^m B_m^2 \\ +A_m^2 & +(-1)^m A_m^2 & +B_m^2 & +(-1)^m B_m^2 \\ -A_m^1 & -(-1)^m A_m^1 & -B_m^1 & +(-1)^m B_m^1 \end{bmatrix} \begin{bmatrix} a_m \\ a_{-m} \\ b_m \\ b_{-m} \end{bmatrix}$$

Solving easily for a_m, a_{-m}, b_m, b_{-m}.
Note that the incident angle, ϕo, affects only the RHS values. Therefore, ϕ_o can be varied without needing to recalculate the eigenfunctions A^1_m, ...

Finally, for m=0,

$$\tilde{A}_o = a_o A_o^1 - b_o B_o^1$$

$$\tilde{C}_o = a_o B_o^1 + b_o A_o^1$$

as $r \rightarrow r_o$

$$A_0^1 \rightarrow J_o(kr_o)$$

$$\frac{\partial A_o^1}{\partial r} = \left(\frac{\partial (J_o kr)}{\partial r} \right)_{r=r_o}$$

$H(A_o^1) = 0$ and analogously for B_o^1.

APPENDIX D

INFINITELY LONG CIRCULAR CYLINDERS - NORMAL INCIDENCE

I. Formulation

Scattering from an infinitely long cylinder, when the incident field propagates normal to the cylinder axis (taken as the z axis) is essentially a two dimensional problem. This is evident because there is no variation in the incident field or in the cylinder properties in the axial or z direction; hence, the scattered field will not vary in the z direction. The cylinder surface is a natural coordinate surface in this system (i.e., r = a), and boundary value techniques give an exact solution.

The incident wave is considered to be planar, and, in general, is polarized arbitrarily. However, it can be resolved into two components : (1) an E-field component parallel to the cylinder axis, and (2) an E-field perpendicular to the same axis (or an H-field component parallel to the axis). Each case is then treated separately. The two cases will be distinguished by $\parallel$ or $\perp$, or TM and TE, referring to (1) and (2) above respectively. The plane of incidence is considered to be the x-z plane.

Since an electromagnetic field can be expressed entirely in terms of either the electric or the magnetic field, the problems can be solved for

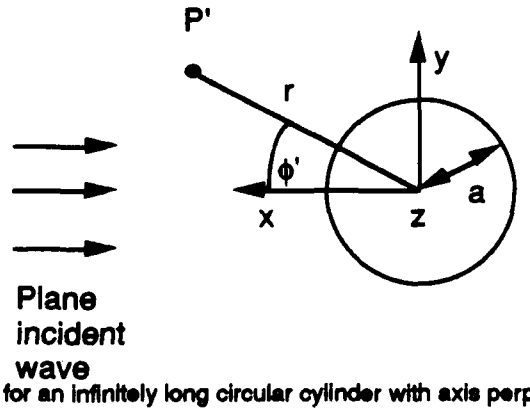

Fig. 1 Scattering geometry for an infinitely long circular cylinder with axis perpendicular to the page.

the two cases by : (a) using only the axial electric field for case (1), and (b) using only the axial magnetic field for case (2). In either case, both the incident and scattered fields posses only axial components. The boundary conditions at the cylinder can be expressed in terms of these axial components, and a scalar problem rather than a vector problem must be solved, which simplifies the solution considerably. (Such is not the case with a sphere, because the incident field strikes the sphere at different angles corresponding to different points on the sphere; hence, that problem retains a vector nature.)

Consider the incident wave to be resolvable into components of the form

$$E^i = e^{-ik_0x}\begin{Bmatrix} E^i_{\parallel}\hat{z} \\ E^i_{\perp}\hat{\phi} \end{Bmatrix} \qquad (d.1)$$

where the field is incident from the left in figure 1. The scattered field at point P' can be expressed for each of the above two scalar field components as

$$E^s_{\parallel}(P') = E^i_{\parallel}\sum_{n=0}^{\infty}(-i)^n\varepsilon_n A_n H_n^{(1)}(k_0r)\cos(n\phi') \qquad (d.2)$$

$$H^s_{\perp}(P') = H^i_{\perp}\sum_{n=0}^{\infty}(-i)^n\varepsilon_n B_n H_n^{(1)}(k_0r)\cos(n\phi') \qquad (d.3)$$

and

where

$$H^i_{\perp}(P') = -\frac{1}{\eta}E^i_{\perp}$$

and

$$\varepsilon_n = \begin{cases} 1 & \text{for } n = 0 \\ 2 & \text{for } n = 1,2,3,\ldots \end{cases}$$

In the above equations, $H_n^{(1)}(k_0r)$ is a cylindrical Hankel function of the first kind of order n and argument k_0r; it has

the proper behavior large r corresponding to the time convention used here. The constants A_n and B_n are functions only of the cylinder material and radius, and are given in following sections for the cylinder type considered. It is again pointed out that in case (1), both the incident and scattered electric fields are polarized parallel to the cylinder axis; while in case (2), the incident and scattered magnetic fields are polarized parallel to the axis.

II. Far-Zone Simplification and Scattering Width

Simplification of the above series solution is possible when (i) $k_o r >> (k_o r)^2$ and (ii) $k_o r >> 1$ (or $r >> \lambda_o$). In this case, a large-argument expansion can be used for the Hankel function. That is

$$E_{\parallel}^{s}(P') = E_{\parallel}^{i} \sqrt{\frac{2}{\pi}} \frac{e^{i\left(k_o r - \frac{\pi}{4}\right)}}{\sqrt{k_o r}} T_{\parallel}(\phi') \qquad (d.4)$$

$$H_{\perp}^{s}(P') = H_{\perp}^{i} \sqrt{\frac{2}{\pi}} \frac{e^{i\left(k_o r - \frac{\pi}{4}\right)}}{\sqrt{k_o r}} T_{\perp}(\phi') \qquad (d.5)$$

where

$$T_{\parallel}(\phi') = \sum_{n=0}^{\infty} (-1)^n \varepsilon_n A_n \cos(n\phi') \qquad (d.6)$$

and

$$T_{\perp}(\phi') = \sum_{n=0}^{\infty} (-1)^n \varepsilon_n B_n \cos(n\phi')$$

In contrast with the exact Mie series for far-zone scattering from a sphere, the field from an infinite cylinder decreases as $1/\sqrt{r}$, rather than the $1/r$ dependence for objects of finite dimensions, such as spheres. Such must be the case in

order for the total energy in the diverging scattered fields to be conserved.

$$\sigma_{\parallel}^{c}(\phi') = \frac{4}{k_0} \left| T_{\parallel}(\phi') \right|^2 \qquad \text{(d.7)}$$

and

$$\sigma_{\perp}^{c}(\phi') = \frac{4}{k_0} \left| T_{\perp}(\phi') \right|^2$$

Two special scattering directions give further simplification :

(a) *Backscattering.* Here , $\phi' = 0$, and the above results simplify

$$T_{\parallel}(0) = \sum_{n=0}^{\infty} (-1)^n \varepsilon_n A_n \qquad \text{(d.8)}$$

and

$$T_{\perp}(0) = \sum_{n=0}^{\infty} (-1)^n \varepsilon_n B_n$$

The backscattering widths become

$$\sigma_{\parallel}^{c}(0) = \frac{4}{k_0} \left| \sum_{n=0}^{\infty} (-1)^n \varepsilon_n A_n \right|^2$$

and

$$\sigma_{\perp}^{c}(0) = \frac{4}{k_0} \left| \sum_{n=0}^{\infty} (-1)^n \varepsilon_n B_n \right|^2$$

(b) *Forward Scattering.* Here, $\phi' = \pi$, and the scattering amplitudes simplify to

$$T_{\parallel}(\pi) = \sum_{n=0}^{\infty} \varepsilon_n A_n$$

and

$$T_{\perp}(\pi) = \sum_{n=0}^{\infty} \varepsilon_n B_n$$

The forward scattering widths then become

$$\sigma_{\parallel}^{c}(\pi) = \frac{4}{k_0} \left| \sum_{n=0}^{\infty} \varepsilon_n A_n \right|^2$$

and

$$\sigma_{\perp}^{c}(\pi) = \frac{4}{k_0} \left| \sum_{n=0}^{\infty} \varepsilon_n B_n \right|^2$$

III. Perfectly Conducting Cylinder

The coefficients A_n and B_n appearing in the exact solution for the perfectly conducting infinitely long cylinder at normal incidence are

$$A_n = -\frac{J_n(k_0 a)}{H_n^{(1)}(k_0 a)}$$

and

$$B_n = -\frac{J_n'(k_0 a)}{H_n^{(1)\prime}(k_0 a)}$$

where the primes represent derivatives with respect to the expressed argument. $J_n(k_0 a)$ is the usual cylindrical Bessel function of order n and argument $k_0 a$. These coefficients are easily generated on a computer by recurrence techniques, or are found in the tables.